

# Trimethoxybenzanilide-Based P-Glycoprotein Modulators: An Interesting Case of Lipophilicity Tuning by Intramolecular Hydrogen Bonding

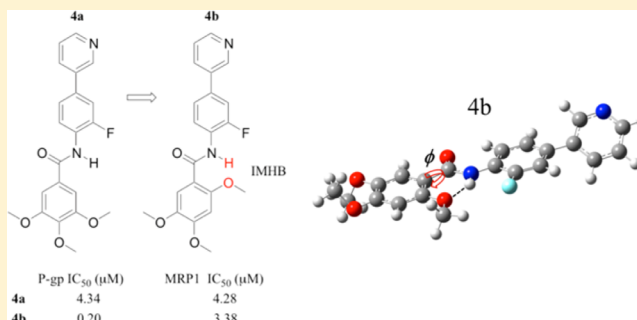
Piero Tardia,<sup>†</sup> Angela Stefanachi,<sup>†</sup> Mauro Niso,<sup>†</sup> Diana Antonella Stolfi,<sup>†</sup> Giuseppe Felice Mangiatordi,<sup>†</sup> Domenico Alberga,<sup>‡</sup> Orazio Nicolotti,<sup>†</sup> Gianluca Lattanzi,<sup>‡</sup> Angelo Carotti,<sup>†</sup> Francesco Leonetti,<sup>†</sup> Roberto Perrone,<sup>†</sup> Francesco Berardi,<sup>†</sup> Amalia Azzariti,<sup>§</sup> Nicola Antonio Colabufo,<sup>\*,†</sup> and Saverio Cellamare<sup>\*,†</sup>

<sup>†</sup>Dipartimento di Farmacia—Scienze del Farmaco, Università di Bari "Aldo Moro", Via Orabona 4, 70125 Bari, Italy

<sup>‡</sup>Dipartimento di Fisica, Università di Bari "Aldo Moro", INFN & TIRES, Via Amendola 173, 70126 Bari, Italy

<sup>§</sup>Clinical and Preclinical Pharmacology Laboratory, National Cancer Research Centre, Istituto Tumori Giovanni Paolo II, Viale O. Flacco 65, 70124 Bari, Italy

**ABSTRACT:** One of the principal reasons for the chemotherapy failure is the overexpression of drug efflux pumps, ABCB1 (also known as MDR1 or P-gp) and ABCC1 (also known as MRP1), whose inhibition remains a priority to circumvent drug resistance. We have recently shown a clear trend between lipophilicity and P-glycoprotein inhibitory activity for a class of galloyl-based modulators targeting P-glycoprotein and MRP1. Herein we report a new series of polymethoxy benzamides, whose lipophilicity was modulated through the establishment of an intramolecular hydrogen bond (IMHB) which allows reaching of P-gp inhibitory activity at the submicromolar IC<sub>50</sub> level. The present study provides a strong rationale for candidates in the presence of IMHB as a key element for a high P-gp inhibitory activity.



## INTRODUCTION

The multidrug resistance (MDR) of cancer consists in an acquired lack of sensitivity to anticancer drugs. It is translatable to a "self-defense" mechanism occurring in numerous kinds of malignant cells, of blood and solid tumors, after their exposure to antineoplastic treatment.<sup>1</sup>

ABCB1 (P-gp, p-glycoprotein) and ABCC1 (multidrug resistance associate protein 1, MRP1) are members of the ubiquitous ATP-binding cassette (ABC) superfamily, physiologically expressed at the blood–brain barrier (BBB), the blood–cerebrospinal fluid barrier (B-CSF), and the intestinal barrier, thus modulating the uptake and the elimination of drugs and toxins.<sup>2,3</sup>

One of the best characterized ABC proteins is P-gp, an ~170 kDa mammalian glycoprotein that is a polyspecific multidrug efflux pump<sup>4,5</sup> and whose overexpression in the plasma membrane of tumor cells contributes to MDR.<sup>6,7</sup>

P-gp substrates are typically amphipathic, and there is a considerable evidence that their interaction with the protein occurs within the plasma membrane either at the extracellular or cytoplasmic side.<sup>2,4</sup>

A recently solved X-ray crystal structure of P-gp shows an open, easily accessible region at the cytoplasmic side. This suggests that drugs may enter into that pocket through the inner membrane leaflet.<sup>8</sup> As a consequence, it may be postulated that

the P-gp transporter activity is profoundly affected by the ability of the ligands to cross the cellular membrane depending in turn by their physicochemical properties. Despite the recent advances in the ADME-tox optimization, further efforts are needed to address the P-gp activity of new potential drug candidates for CNS pathologies.<sup>9</sup> In the past two decades, a number of P-gp modulators spanning a wide range of chemical diversity have been designed and studied in depth.<sup>10</sup> Some of them have entered phase III clinical trials, but none of them has been approved so far for clinical use because of their serious side effects and lack of sufficiently proved efficacy.<sup>3</sup>

The compelling goal, of covering those gaps, is challenging the scientific community and new strategies are being exploited.<sup>11</sup> Notably, the attrition toward an expedite progression is determined by the lack of adequate structural information on the target(s), which is necessary for rationally tuning molecular activity and selectivity and reducing side effects.<sup>12</sup> However, a firm notion based on structure–activity relationship (SAR) and quantitative structure–activity relationship (QSAR) studies is that high lipophilicity is necessary to achieve significant P-gp activity.<sup>13</sup> This concept was highlighted in some recent studies, indicating an entry pathway through the membrane bilayer.<sup>4</sup>

**Received:** February 21, 2014

**Published:** July 20, 2014

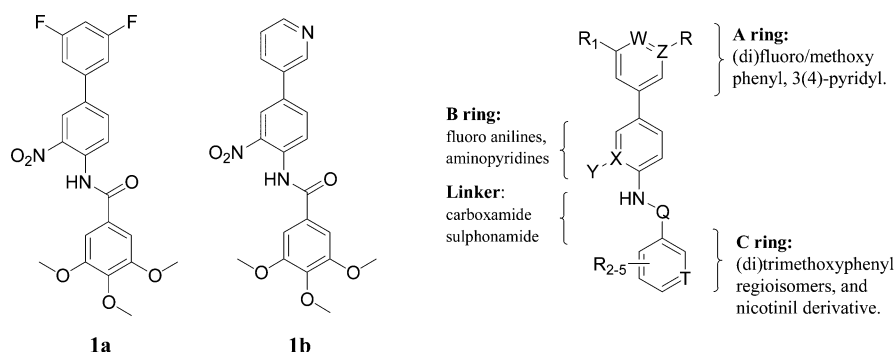


Figure 1.

Indeed, in our recent work on galloyl-based selective modulators of MDR1 and P-gp,<sup>14</sup> we envisaged a certain correlation between lipophilicity and the ability of modulating P-gp. For instance, compound **1a** (Figure 1), having the highest dual P-gp/MRP1 inhibitory potency, was also the most lipophilic of the series, even if, unexpectedly, its pyridyl congener **1b** was only three times less active despite its much higher water solubility, as assessed by turbidimetric assay<sup>15</sup> (**1a**,  $0.005 \pm 0.003$  mg/L; **1b**,  $10 \pm 2$  mg/L).

Building on this work, we planned the design, synthesis, and biological evaluation of a new series of dual P-gp/MRP1 *N*-biphenyl-benzamide inhibitors with an improved physicochemical profile (solubility, lipophilicity, etc.) and lacking the liable nitro group. In particular, the lipophilicity was modulated also by synthesizing a number of trimethoxyphenyl regioisomers with diverse propensity to form intramolecular hydrogen bond.<sup>16–18</sup>

The new molecular panel was built by assembling the three aromatic rings depicted in Figure 1 (rings A, B, and C), namely a (di)fluorophenyl, a pyridyl, and a (di)trimethoxyphenyl moiety, respectively, through a carboxamide or a sulphonamide group linking B to C.

In doing so, we prepared a new series of 21 biologically active P-gp inhibitors having activity values reaching submicromolar IC<sub>50</sub> level (Table 1). Eleven out of 21 compounds acted as inhibitors on both P-gp and MDR1 with some very interesting IC<sub>50</sub> values.

## CHEMISTRY

The synthetic pathways chosen for the preparation of the designed compounds are shown in Scheme 1, and the obtained compounds are listed in Table 1. In the molecular design, a number of substituents were selected to explore a wide range of stereoelectronic and lipophilic properties. In brief, the starting (hetero)arylanilines (**1–6**, Scheme 1) (“A + B” nuclei) were obtained by Suzuki coupling between the appropriate (hetero)-aniline and the corresponding arylboronic acids. The end products (“A + B + C”) were prepared by coupling the suitable “A + B” nuclei with the appropriate (hetero)aryl- (or sulfonyl-) chlorides, affording the corresponding compounds **2a**, **2b**, **3a**, **3b**, **4a–i**, **5a**, **5b**, **6b**, and **7j** (Scheme 1).

Each compound is identified by a number, referring to the biphenyl system (“A + B” moiety), and a letter corresponding to a specific (hetero)aryl (C). For instance, **2a** and **2b** are 3,4,5- and 2,4,5-trimethoxybenzoyl regioisomers, respectively, as well as **3a** and **3b** and so on.

Starting from **1a**, the reduction of the nitro group provided the amino congener **8a** that was coupled with *N*-acetyl-L-alanine to afford **9a**.

To assess the importance of intramolecular hydrogen bond formation between ring B and ring C of the molecule, we performed the *N*-methylation of amides **4a** and **4b** by treatment with sodium hydride and methyl iodide, affording compounds **10a** and **10b**, respectively. The sulfonamide **7j** was prepared to study the effect of nonclassic bioisosteric replacement on compound **4e**.

**Lipophilicity Studies.** There is good agreement that P-gp activity is strongly influenced by lipophilicity as recently reported for a series of benzophenone-type inhibitors.<sup>12</sup> On the basis of this evidence, we first tried to correlate the calculated log *P* values with pIC<sub>50</sub> values (P-gp inhibition) of our compounds. To this purpose, different programs (BioLoom version 1.5, ACD/Laboratories version 6.00 and ALOGPS v. 2.1) were used. For the sake of clarity, the log *P* values shown in Table 1 and Figure 2 are those given by ALOGPS.<sup>20</sup>

As shown in Figure 2, our expectations were not met as no correlation was observed between activity at P-gp and lipophilicity. It is worth noting that the lack of correlation may be due also to the poor ability of the used software to detect different lipophilicity for the differently substituted methoxy regioisomers and also a different lipophilicity arising from the possible formation of intramolecular hydrogen bonding for some of the examined compounds.

To overcome these drawbacks, we have thus experimentally measured both log *D* values by octanol/pH 7.4 phosphate buffer partitioning<sup>21</sup> and log *k'* as an additional lipophilicity index, determined by HPLC using a reversed stationary phase in isocratic conditions.<sup>22</sup>

As expected, poor correlations between calculated log *P* and log *D*/log *k'* (parts a and b of Figure 3, respectively) were found while a higher correlation was seen between the two experimental parameters log *D* and log *k'* (Figure 3c). Interestingly, the differences between regioisomers of the trimethoxy phenyl ring in terms of lipophilicity such as **2a** vs **2b**, **3a** vs **3b**, **4a** vs **4b**, **5a** vs **5b**, and **10a** vs **10b** (highlighted in red in the plot) can be easily appreciated.

Finally, a significant increase of the determination coefficient (*r*<sup>2</sup>) was observed when considering the relationship between log *D* and pIC<sub>50</sub>. This clearly indicates that also in the series of our *N*-biphenyl-benzamides, P-gp inhibition increases along with the molecular lipophilicity (Figure 3d).

Interestingly, three compounds (**4b**, **5b**, and **3b**), all bearing 2,4,5-trimethoxyphenyl nucleus (C ring), were the most active ones against P-gp although they did not show the highest lipophilicity. This result could be interpreted by considering the presence of an intramolecular hydrogen bond between the 2-

Table 1. Chemical Structure, Lipophilicity, and Biological Activity of Compounds 2a,b, 3a,b, 4a–i, 5a,b, 6b, 7j, 8a, 9a, and 10a,b (The PBS Buffer Solubility Measurements Are Given Only for the Compounds 4a–i)

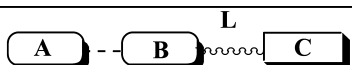
<div style="text-align: center;">  <p>General Picture</p> </div>										
Cpd	A	B	L	C	P-gp <sup>a</sup>	MRP1 <sup>a</sup>	logP <sup>b</sup>	logD <sup>c</sup>	logk <sup>td</sup>	Sol. mg/L <sup>e</sup>
2a					1.30±0.1	5.80±0.41	3.75±0.44	3.59	0.32	
2b					0.97±0.12	>100	3.80±0.46	3.66	0.47	
3a					8.21±0.62	13.60±1.51	2.35±0.39	2.39	-0.44	
3b					0.54±0.09	6.26±0.34	2.39±0.39	3.03	-0.12	
4a					4.34±0.53	4.28±0.34	2.98±0.60	2.48	-0.36	25±3
4b					0.20±0.04	3.38±0.24	3.03±0.58	2.84	0.24	30±4
4c					0.67±0.08	>100	2.97±0.60	3.99	0.37	45±2
4d					2.93±0.28	>100	3.14±0.58	2.38	-0.39	60±3
4e					8.92±0.86	>100	3.15±0.47	2.23	-0.45	18±3
4f					3.30±0.53	>100	3.25±0.43	2.81	-0.18	20±3
4g					5.26±0.77	>100	3.36±0.32	2.9	-0.32	22±5
4h					9.20±1.11	>100	3.41±0.32	2.83	-0.38	40±5
4i					60.10±3.64	>100	2.28±0.32	1.97	-0.68	300±15
5a					3.20±0.63	2.20±0.13	2.98±0.61	2.75	-0.31	
5b					0.31±0.08	>100	3.03±0.59	3.13	0.31	

Table 1. continued

<div style="text-align: center;">  General Picture </div>										
Cpd	A	B	L	C	P-gp <sup>a</sup>	MRP1 <sup>a</sup>	logP <sup>b</sup>	logD <sup>c</sup>	logk <sup>d</sup>	Sol. mg/L <sup>e</sup>
6b					1.23±0.44	>100	4.06±0.63	3.64	0.67	
7j					67.5±3.82	94.50±7.82	2.87±0.52	1.70	-0.88	
8a					2.76±0.65	15.80±2.12	3.63±0.46	2.62	-0.09	
9a					18.50±1.54	11.10±0.98	3.00±0.85	2.31	-0.03	
10a					6.66±1.03	8.13±0.96	3.21±0.58	2.32	-0.51	
10b					21.60±3.01	23.60±2.87	3.26±0.57	1.75	-0.59	
MC18 <sup>f</sup>					1.02±0.14					
Verapamil <sup>f</sup>						3.50±0.34				

<sup>a</sup>The IC<sub>50</sub> data (Calcein-AM assay), reported as  $\mu\text{M} \pm \text{SEM}$ , are averaged over two independent experiments, sampled in triplicate. <sup>b</sup>Calculated by ALOGPS 2.1.<sup>19,20</sup> <sup>c</sup>log D pH 7.4 measurements by Analiza Inc.<sup>21</sup> <sup>d</sup>Logarithm of the capacity factors measured by RP-chromatography using methanol/pH 7.4 phosphate buffer 70:30 as an eluent.<sup>22</sup> <sup>e</sup>Solubility measured by turbidimetric assay.<sup>15</sup> <sup>f</sup>Reference compounds.<sup>28</sup>

methoxy group on the ring C of compounds **4b**, **5b**, and **3b** and the NH group on the ring B.

**Intramolecular Hydrogen Bonds Detection by NMR Studies.** To validate our hypothesis on the intramolecular hydrogen bond (IMHB) as a key element for a high P-gp inhibitory activity, a spectrometric analysis by <sup>1</sup>H NMR was carried out by measuring the chemical shift of one exchangeable NH proton at a single and at variable temperature.

Generally, an exchangeable NH proton that is involved in a HB interaction is more deshielded (higher  $\delta$  chemical shift value, Figure 4a) than a similar, not hydrogen bonded, exchangeable NH proton. As a consequence, a comparative analysis of the chemical shift between two model compounds, namely a sample (3,4,5-trimethoxybenzamide, **4a**) and a control (2,4,5-trimethoxybenzamide, **4b**), was carried out to demonstrate the existence of an IMHB between the NH and the oxygen of the 2-methoxy group in **4b** and not in **4a**.

To confirm the presence of such a IMHB, two different series of experiments were performed on the two selected regioisomers: (i) an eight point <sup>1</sup>H NMR chemical shift determination of the NH exchangeable protons as a function of temperature boost (Figure 4b–c), and (ii) a 2D-<sup>1</sup>H-NOESY assessment (Figures 5a,b).

Because the amide hydrogen involved in IMHB (**4b**) might be more deshielded than the analogue proton unable to form IMHB (**4a**), the <sup>1</sup>H chemical shifts of the NH were measured and

compared in both regioisomers, nicely confirming our expectations (Figure 4a).

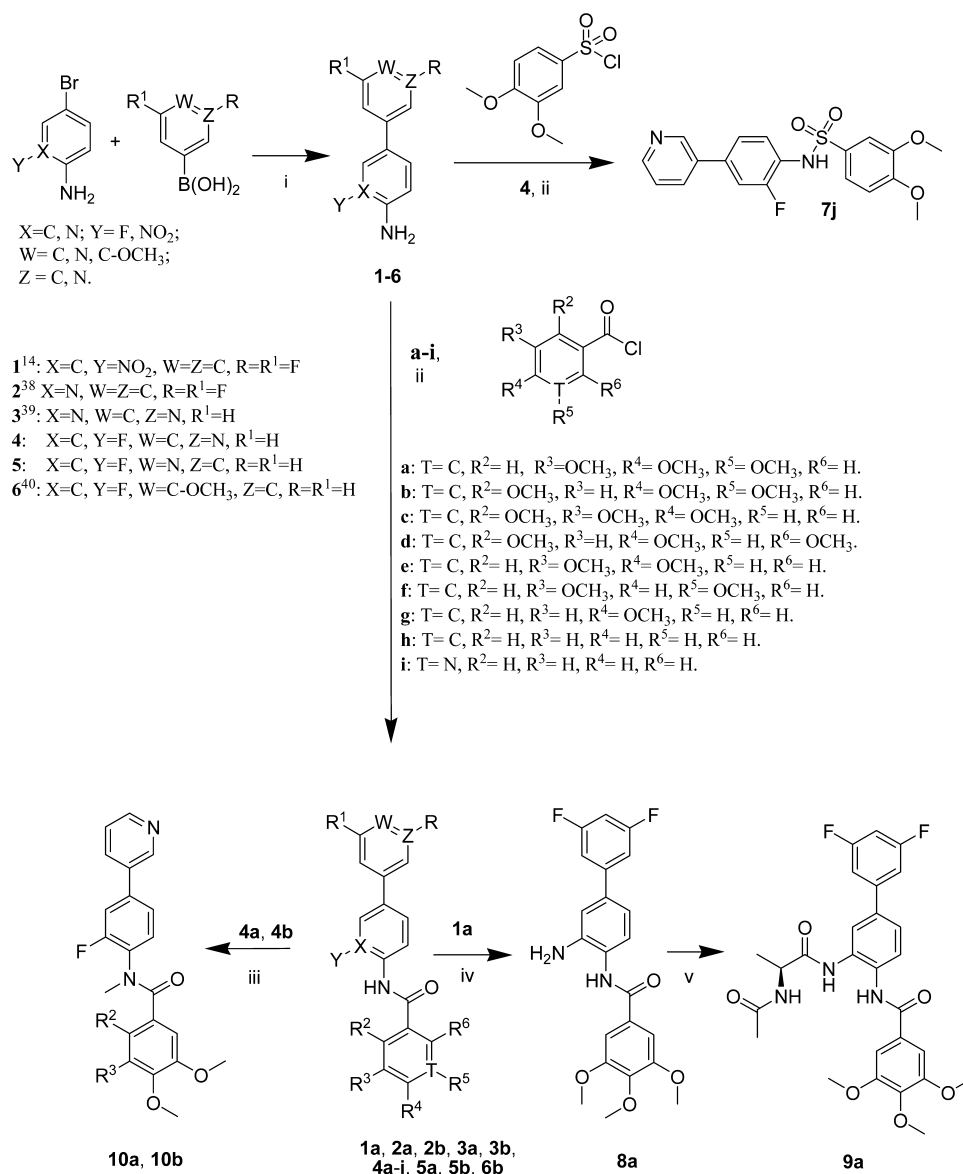
As already described in literature, changes in <sup>1</sup>H chemical shift of exchangeable protons with temperature can be used to determine the presence of IMHB in small molecules.<sup>23</sup>

The temperature coefficient TC was used to evaluate the temperature effect. TC value corresponds to the slope of the line obtained plotting the chemical shift versus the temperature of the experiment (Figure 4b); this value is generally negative and compounds with IMHB exhibit a less negative TC than compounds unable to form IMHB (control, compound **4a**), as in our experiments (Figure 4c).

This means that the  $\Delta\delta$  of the benzamide NH for compound **4b** is less pronounced than for **4a**, accordingly to temperature increase. Evidence of IMHB were also obtained with 2D NOESY experiments, as shown in Figure 5a,b.

We focused our attention on the interactions between the NH proton and the trimethoxyphenyl moiety of both compounds **4a** and **4b**. In the case of compound **4a**, the distance between the amidic proton ( $H^a$ , s, 10.32 ppm) and the meta methoxy substituents ( $H^c$ , s, 3.86 ppm) does not allow the NOE, therefore the only detectable cross pick is the one from the interaction with the in ortho position protons ( $H^b$ , s, 7.36 ppm). In the spectrum of **4b**, as expected, is present the cross pick of the NH ( $H^a$ , s, 10.42 ppm) and the ortho methoxy protons ( $H^f$ , s, 4.06 ppm).

**Scheme 1.** Synthesis of (Hetero)arylanilines 1–6, Dimethoxybenzenesulfonamide 7j, Benzamide 4h, 4-Methoxybenzamide 4g, Dimethoxybenzamides 4e,f Trimethoxybenzamide Derivatives 1a, 2a,b, 3a,b, 4a–d, 5a,b, 6b, 8a, 9a, 10a,b, and Nicotinamide 4i<sup>a</sup>



<sup>a</sup>Reagents and conditions: (i)  $Pd(PPh_3)_4$ , aq  $K_2CO_3$  (2M), 1,4-dioxane, reflux, **Y**: **2** (45%), **3** (50%), **4** (90%), **5** (40%), **6** (30%); (ii) THF dry, room temp, overnight, **Y**: **2a** (23%), **2b** (37%), **3a** (10%), **3b** (68%), **4a** (81%), **4b** (79%), **4c** (56%), **4d** (10%), **4e** (84%), **4f** (98%), **4g** (69%), **4h** (98%), **4i** (77%), **5a** (54%), **5b** (58%), **6b** (87%), **7j** (61%); (iii) NaH,  $CH_3I$ , DMF dry, 0 °C → room temp, 3 h, **10a** (68%), **10b** (19%); (iv) Pd/C (5% w/w) under  $H_2$  atmosphere, absolute ethanol, room temp, 2 h, **8a** (91%); (v) *N*-acetyl-L-alanine, EDC, HOBT, TEA, THF dry, room temp, 72 h, **9a** (32%). **a** = 3,4,5-trimethoxybenzoyl chloride; **b** = 2,4,5-trimethoxybenzoyl chloride; **c** = 2,3,4-trimethoxybenzoyl chloride; **d** = 2,4,6-trimethoxybenzoyl chloride; **e** = 3,4-dimethoxybenzoyl chloride; **f** = 3,5-dimethoxybenzoyl chloride; **g** = 4-methoxybenzoyl chloride; **h** = benzoyl chloride; **i** = nicotinoyl chloride.

## ■ COMPUTATIONAL STUDIES

To evaluate the influence of the IMHB on the conformation of the investigated molecules, molecular dynamics simulations were carried out on regioisomers **4a** and **4b**. The analysis was performed by considering the molecules fully solvated either in water or in chloroform, the latter representing one of the organic solvents used to model the membrane environment in MD simulations.<sup>24,25</sup> The probability distribution of the values of the dihedral angle  $\varphi$  ( $P(\varphi)$ ), indicating the system planarity (see Figure 6c), were taken into account. As depicted in parts a and b of Figure 6, at variance with compound **4a** displaying two different stable conformations (corresponding to  $\varphi = 30^\circ$  and  $\varphi$

$= 150^\circ$ ) only one, planar conformation, is observed for **4b** ( $\varphi = 180^\circ$ ). Importantly, such difference is more evident when the solvent is chloroform rather than water, thus suggesting that the effect of the H-bond on the planarity is enhanced when the molecule permeates through the membrane. We found an increased stability of the intramolecular hydrogen bond in chloroform when compared to water. This effect is significant because it contributes to the planarity of the molecule in a lipophilic environment, which facilitates the passage through membrane.

The strength of hydrogen bonds ranges energies enabling even short-lived association and dissociation under ambient con-



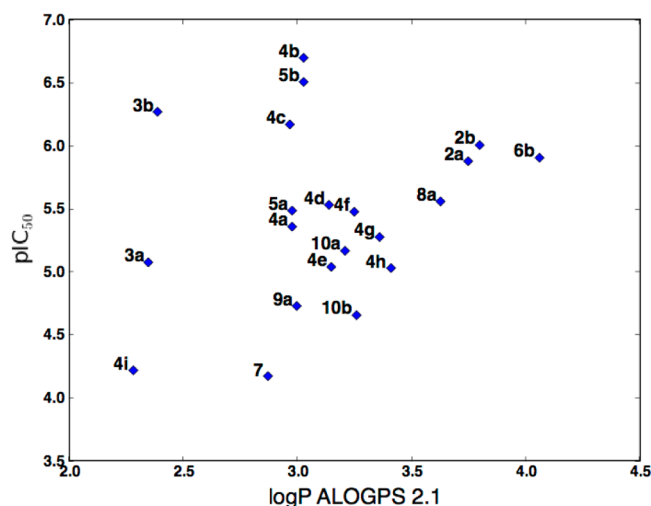


**Figure 2.** Relationship between P-gp inhibitory potency of compounds listed in Table 1 (expressed as  $pIC_{50}$  values) and calculated log  $P$  values (ALOGPS).

ditions. It goes without saying that the role of intramolecular and intermolecular hydrogen bonding is relevant, not only for the recognition mechanism and stabilization of a preferred conformation but also for the improvement of several physicochemical properties such as the permeability.

In this respect, it has been recently demonstrated<sup>18</sup> that the occurrence of intramolecular hydrogen bonds can affect several *in vitro* properties determining higher lipophilicity and cell permeability.

Another relevant study,<sup>26</sup> emphasized how the formation of intramolecular hydrogen bonds in drug molecules can shield the polarity and thus improve lipophilicity. Thus, our design of compounds having the chance of forming an intramolecular hydrogen bond (IMHB) is important to bias closed planar conformation shielding the polarity relative to that open with a gain in lipophilicity and, more importantly, in the permeation of biological membranes.

Finally, density functional theory (DFT) calculations were also performed in order to compute the HB breaking energy barrier required in **4b**. A relaxed scan calculation (level of theory B3LYP/6-31G(d)) was carried out in order to build a complete picture of the potential energy profile for the torsion around the dihedral angle  $\varphi$  (Figure 6d).

The obtained data confirm that the IMHB is highly stable, being the required energy barrier higher than 10 kcal/mol. Following the same approach, the IMHB breaking energy barriers were computed for all those compounds for which an IMHB could be predicted, namely **2b**, **3b**, **4b**, **4c**, **4d**, **5b**, and **6b**. The obtained data (including the energy barrier already calculated for compound **4b**) confirm the occurrence of a stable IMHB in these compounds and, more importantly, disclose a pretty correlation with the  $IC_{50}$  values ( $r^2 = 0.960$ , see Figure 7). Satisfactorily, DFT energy barrier values are valuable observables for a fine-tuning molecular design as they allow accurate discrimination of even small structural variations of highly active compounds,  $IC_{50}$  ranging from 0.20 to 2.93  $\mu$ M (see Figure 7 and Table 1). It is worth noting that a good correlation ( $r^2 = 0.788$ ) persists even in absence of **4d**, a possible influential outlier. In summary, both MD simulations and DFT calculations suggest the presence of a unique conformation of **4b** characterized by a very stable IMHB, thus providing a solid molecular rationale for

the different activities reported for the regioisomers **4a** and **4b**. The strength of such interaction is here proved to be a sensitive parameter for a soft modulation of the P-gp response. For instance, the 2,4,5-trimethoxybenzamide derivatives **3b**, **4b**, and **5b** display the highest activity and are also characterized by the strongest IMHB.

## BIOCHEMICAL STUDIES

**Calcein-AM Experiment.** P-gp and MRP1 modulating activities of tested compounds were determined by fluorescence measurements, using calcein-AM fluorescent probes, in MDCK-MDR1 and MDCK-MRP1 cell lines.<sup>27</sup> These cells overexpress only P-gp or MRP1 transporters, respectively, so that the observed biological effects can be ascribed to the specific inhibition of these pumps. Calcein-AM is a lipophilic substrate of both P-gp and MRP1, able to cross the cell membrane. Inside the cell compartment, it is hydrolyzed by endogenous cytoplasmic esterases, yielding highly fluorescent calcein. This compound is not a P-gp or MRP1 substrate, and it cannot cross the cell membrane via passive diffusion because it is too hydrophilic. Thus, a rapid increase in the fluorescence of cytoplasmic calcein can be monitored. P-gp and MRP1 transporters, expressed in the cell membrane, rapidly efflux the calcein-AM before its entrance into the cytosol, giving a reduction of the fluorescent signal due to a decrease in the accumulation of calcein. Evaluation of P-gp or MRP1 activity in the presence of pump inhibitors can be performed in a competitive manner.

Compounds that block P-gp and MRP1 pumps inhibit calcein-AM efflux, increasing intracellular accumulation of fluorescent calcein. Values of  $IC_{50}$  for calcein-AM uptake (Table 1) were determined by measuring relative fluorescence values obtained after 30 min of incubation at 37 °C. Typical sigmoidal dose-response curves, regarding MRP1 activity, are shown in Figure 8 in the presence of various concentrations of selected MRP1 and P-gp inhibitors such as Verapamil and MC18<sup>28</sup> were used as reference compounds for MRP1 and P-gp inhibition, respectively. The accuracy and reproducibility of the estimated  $IC_{50}$  values are in accordance with the most recent guidelines.

**Anticancer Activity Evaluation through a Co-administration Assay.** To verify doxorubicin activity in resistant MCF7adr cell line, the same antineoplastic drug has been administrated with compounds **2b**, **4b**, **4c**, and **5b** displaying P-gp activity in the submicromolar range. The co-administration assays have been carried out at three different concentrations of selected compounds (Figure 9). The effect of doxorubicin in co-administration has been evaluated after 72 h by MTT test and the results suggest that the block of P-gp ligands, in a dose dependent manner as depicted in each corresponding graph reported in Figure 9, permitted a recovery of the doxorubicin effect with respect to the control.

**Bioluminescent ATP Assay.** To obtain some details in terms of P-gp interacting mechanism, cellular ATP depletion was evaluated in the presence or absence of compounds **2b**, **4b**, **4c**, and **5b** in MDCK-MDR1 (Figure 10). All compounds were unable to deplete ATP and therefore behave as potential P-gp inhibitors. This results permit hypothesizing that tested compounds may be P-gp inhibitors or, alternatively, not detected by P-gp sites. Moreover, these results should be matched with apparent permeability evaluation to prove/confirm this mechanistic hypothesis. In this assay, for each compound both the flux from basolateral to apical ( $B \rightarrow A$ ) and the flux from apical to basolateral ( $A \rightarrow B$ ) were evaluated. The  $B \rightarrow A$  flux represents the passive transport, whereas the flux  $A \rightarrow B$  is the active

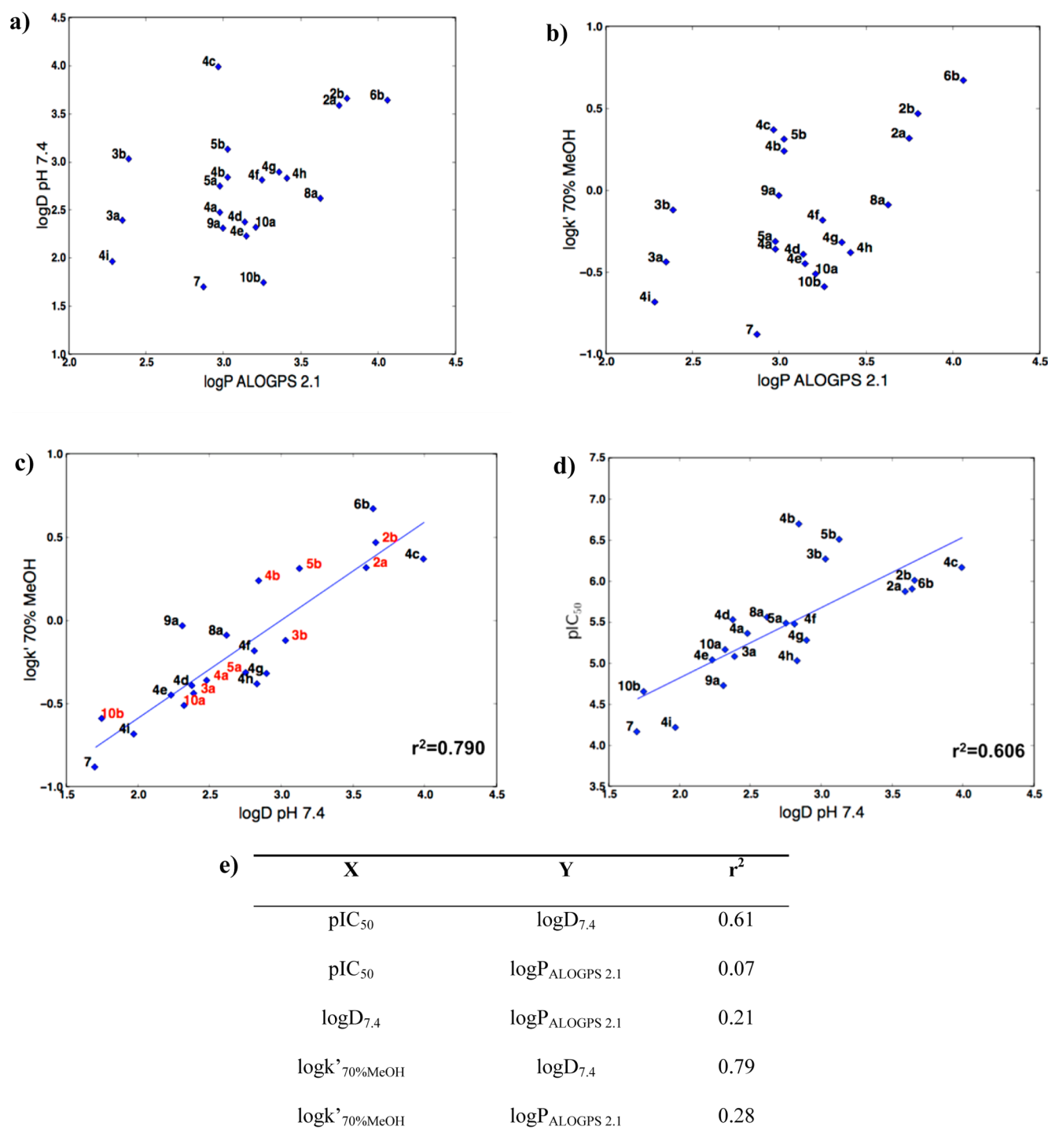


**Figure 3.** (a) Relationships between calculated  $\log P$  and experimental  $\log D_{7.4}$  values; (b) calculated  $\log P$  and experimental  $\log k'_{70\% \text{ MeOH}}$  values; (c)  $\log D_{7.4}$  and  $\log k'_{70\% \text{ MeOH}}$  values; (d)  $\log D_{7.4}$  and P-gp inhibitory potency ( $pIC_{50}$ ) of compounds listed in Table 1; (e) determination coefficient ( $r^2$ ) of correlation between studied theoretical and experimental parameters.

transport. For each tested compound was estimated BA/AB ratio, and compounds displaying BA/AB > 2 are considered P-gp substrates whereas compounds BA/AB < 2 are estimated P-gp inhibitors. Unexpectedly, permeability results indicated that these ligands were P-gp substrates and so this apparent discrepancy with ATP cell depletion results will be addressed later, after the discussion of the experimental permeability data.

**Permeability Experiment.** The apparent permeability ( $P_{\text{app}}$ ) in Caco-2 cell monolayer has been determined for

compounds 2b, 4b, 4c, and 5b. In this experiment, the fluxes of each ligand from basolateral to apical (B → A) and from apical to basolateral (A → B) compartments have been evaluated. The (B → A) flux indicates the role of passive flux of compound, whereas the (A → B) flux displays the active transport because P-gp is localized at apical level. Actually (B → A)/(A → B) ratio permits prediction of whether a ligand could be considered a substrate (ratio >>2) or inhibitor (ratio ≤2) of P-gp.<sup>29</sup> The tested compounds displayed the following (B → A)/(A → B) ratio: 14,

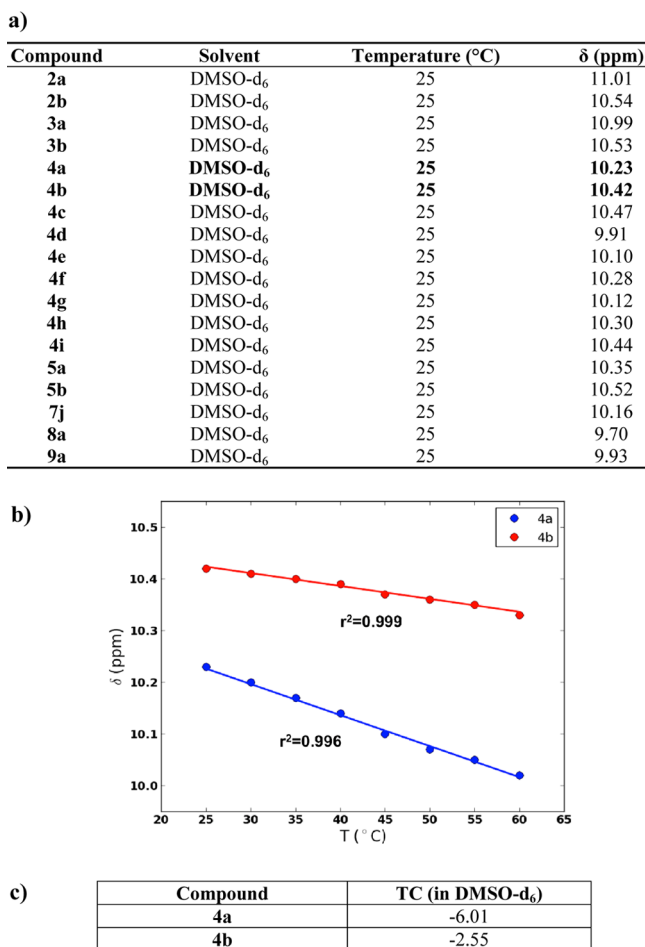


**Figure 4.** (a)  $^1\text{H}$  chemical shifts of exchangeable protons belonging to compounds 2a–9a; (b) plots of the chemical shift vs the temperature; (c) temperature coefficients (TC).

8.1, 6.7, and 10.7 for **4b**, **5b**, **4c**, and **2b**, respectively. These results indicated that all tested compounds could be considered P-glycoprotein substrates. To confirm such a hypothesis, the  $P_{\text{app}}$  was also detected in the presence of MC18, a known P-gp inhibitor. This allowed us to verify the increase of  $A \rightarrow B$  flux. Indeed, for compounds **4b**, **4c**, and **2b**, the BA/AB ratio shifted from 14, 6.7, 10.7 to 8.2, 6.1, and 8.2, respectively, hence confirming that these compounds are “pure” P-gp substrates. All these results are the mean of three independent experiments samples in triplicate. Compound **5b** displayed an out-of-trend result because BA/AB ratio increases from 8.1 to 11.2. This apparent discrepancy could be the result of the ability of this compound to be also a breast cancer resistance protein (BCRP) substrate and so blocks P-gp and stimulates also the BCRP efflux.

## RESULTS AND DISCUSSION

To obtain higher aqueous solubility, a pyridyl moiety was introduced, affording very interesting results in terms of P-gp inhibition.

For example, compounds **4a–i**, which contain the 2-fluorophenyl as B ring and the 3-pyridyl as A ring, showed good aqueous solubility, as assessed by turbidimetric assay (for compounds **4a–4i**, are reported in Table 1),<sup>15</sup> and P-gp activity ranging from 0.2 to 9.2  $\mu\text{M}$ ; the only exception is due to the nicotinamide derivative **4i** ( $\text{IC}_{50}$  60.1  $\mu\text{M}$  on P-gp and  $>100 \mu\text{M}$  on MRP1), probably due to a drop of lipophilicity. The best

result is given by compound **4b** (bearing a 2,4,5-trimethoxyphenyl as C ring), exhibiting a submicromolar and low micromolar inhibitory activity on P-gp and MRP1, respectively ( $\text{IC}_{50}$  0.2  $\mu\text{M}$  on P-gp and 3.38  $\mu\text{M}$  on MRP1). As already discussed, the 2-methoxy group on C ring is able to establish an intramolecular hydrogen bond with the benzamide NH that stabilizes a planar conformation. To detect the optimal substitution pattern needed to ensure a better P-gp inhibition, two new regioisomers of compound **4b** were synthesized, that is, the 2,3,4-trimethoxyphenyl derivative **4c** and 2,4,6-trimethoxyphenyl isomer **4d**. The observed  $\text{IC}_{50}$ s on P-gp are 0.67 and 2.93  $\mu\text{M}$ , respectively and on MRP1 are both  $>100 \mu\text{M}$ .

Indeed, all the 2,4,5-trimethoxybenzoyl derivatives, namely **2b**, **3b**, **4b**, **5b**, and **6b**, showed good inhibition results: **2b** has an  $\text{IC}_{50}$  of 0.97  $\mu\text{M}$  on P-gp and  $>100 \mu\text{M}$  on MRP1; **3b** an  $\text{IC}_{50}$  of 0.54  $\mu\text{M}$  on P-gp and 6.26  $\mu\text{M}$  on MRP1; **5b** an  $\text{IC}_{50}$  of 0.31  $\mu\text{M}$  on P-gp and  $>100 \mu\text{M}$  on MRP1; **6b**, has an  $\text{IC}_{50}$  of 1.23  $\mu\text{M}$  on P-gp and  $>100 \mu\text{M}$  on MRP1. All these compounds showed higher activity than the corresponding 3,4,5-trimethoxybenzoyl regioisomers (named as -a series).

A likely reason can be found in the occurrence of an IMHB, which is established from the methoxy group at the 2-position of the C ring and the benzamide NH. Interestingly, such IMHB is responsible for the adoption of a molecular conformation whose polar content is decreased so that they could shed water in the presence of a low dielectric environment like a hydrophobic phospholipid bilayer.<sup>30,31</sup>

To confirm this hypothesis, the synthesis of the *N*-methylated congeners of **4a** and **4b** was carried out, giving compounds **10a** and **10b** respectively, which were supposed to be less active, being unable to establish an IMHB. As expected, while for **4a** and **4b** the observed  $\text{IC}_{50}$ s on P-gp are 4.34 and 0.20  $\mu\text{M}$ , respectively, and on MRP1 4.28 and 3.38  $\mu\text{M}$ , respectively, for compounds **10a** and **10b**, increased  $\text{IC}_{50}$  values on P-gp (6.66 and 21.6  $\mu\text{M}$ , respectively) and on MRP1 (8.13 and 23.6  $\mu\text{M}$  respectively) were obtained.

The bioisosteric replacement of the carboxamide linker “L” in **4e** with a sulfonamide one led to compound **7j**, displaying a decreased activity on P-gp ( $\text{IC}_{50}$  = 8.92 vs 67.5  $\mu\text{M}$ ), likely due to the strongly lowered lipophilicity determined by the more polar and partly ionized sulphonamido linker at pH 7.4.

The reduction in **1a** of the nitro group to the amino derivative **8a** resulted in an increase of activity on P-gp ( $\text{IC}_{50}$  2.76  $\mu\text{M}$ ). Its coupling with *N*-acetyl-L-alanine gave **9a**, showing a lower P-gp inhibition potency ( $\text{IC}_{50}$ : 18.5 and 11.1  $\mu\text{M}$  on P-gp and MRP1, respectively).

Disappointingly, no significant correlation was found between  $\text{pIC}_{50}$  at P-gp and the calculated  $\text{cLogPs}$ ,  $\text{ALogPs}$ , and  $\log D$ s for our series of compounds. The poor correlation is probably due to the inability of the aforementioned predicting methods of assessing the occurrence of intramolecular H-bonds and thus its effect on lipophilicity.

The  $\log D$  experimental data at pH 7.4, on the other hand, showed a still low, but definitely better correlation coefficient, indicating that an increased lipophilicity is generally accompanied by an increased activity (see Figure 3d).

The IMHB showed by some compounds of our series involves the methoxy and NH groups in C- and B-rings, respectively, leading to the formation of a third pseudo-six-membered ring system. When the occurrence of the IMHB is not allowed, the lipophilicity drops dramatically as in case of the tertiary amide **10b** (compare with **4b**). None of the three aforementioned programs was able to predict the difference of  $\log D$  found out



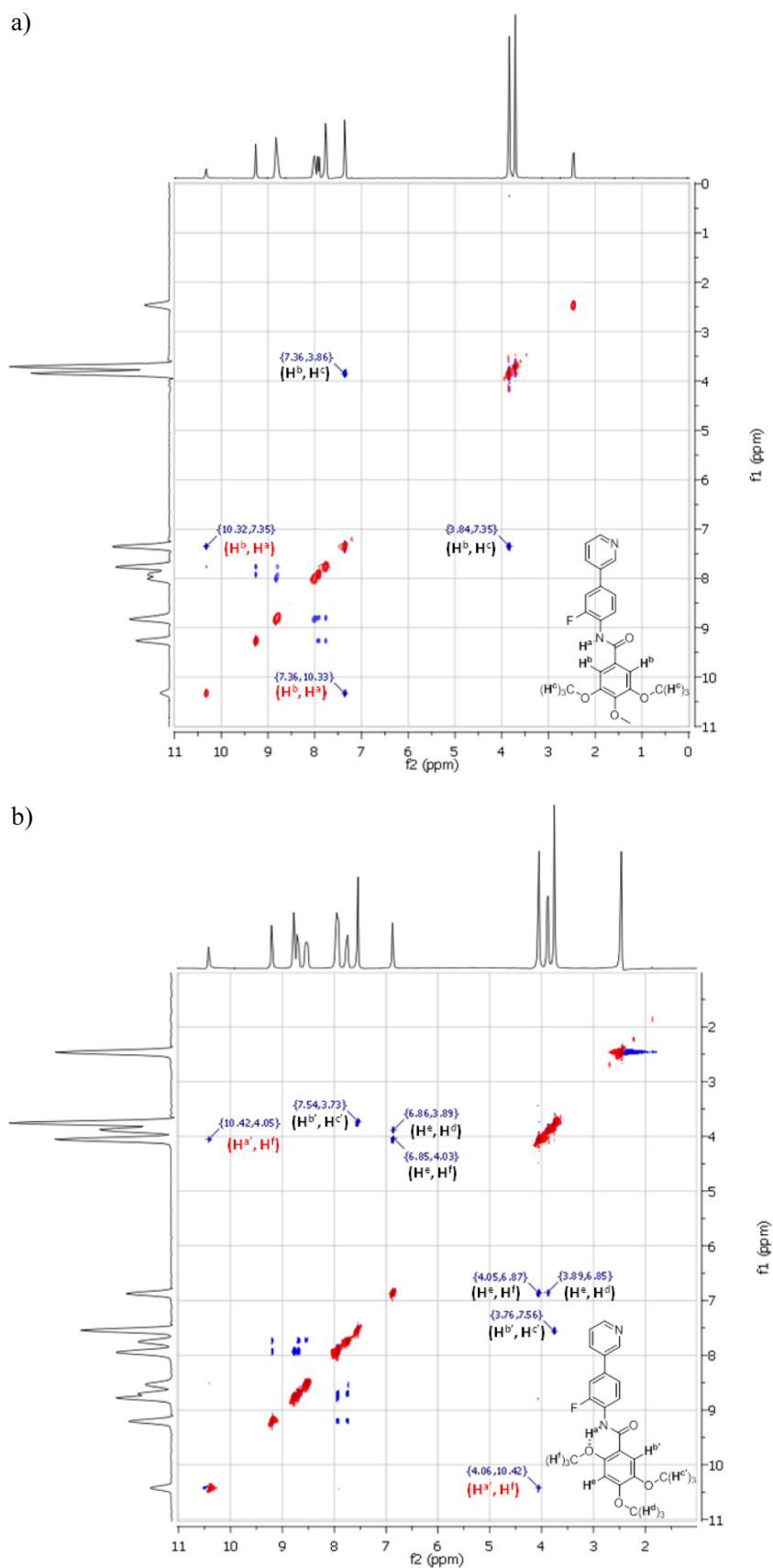
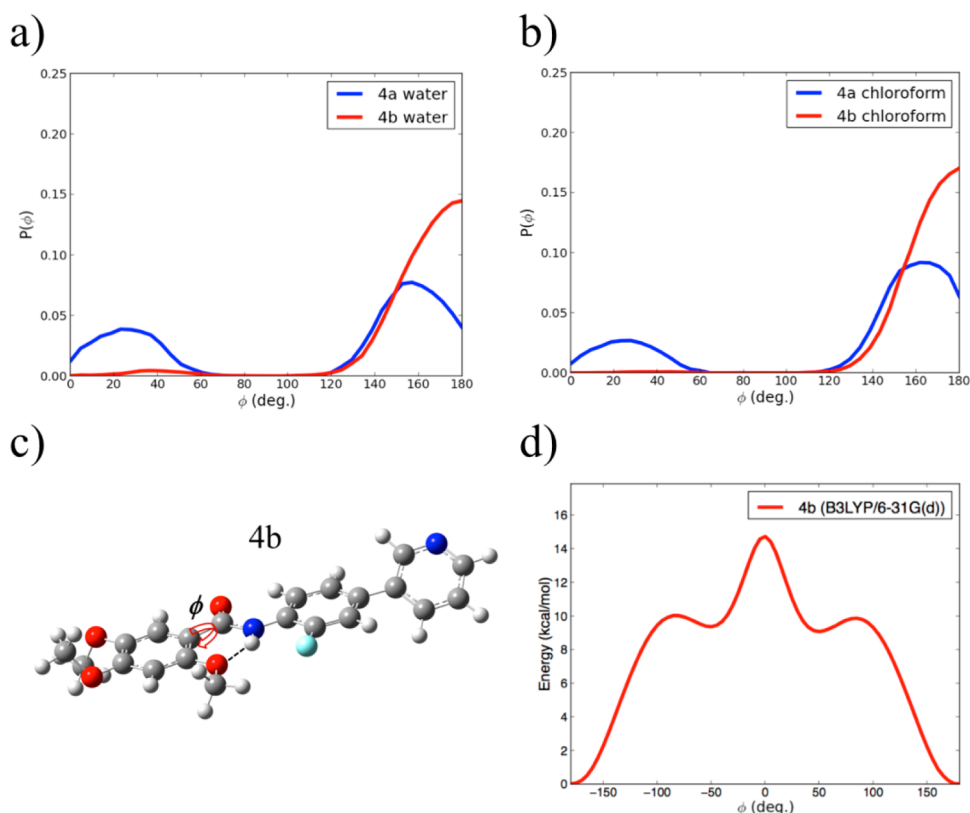


Figure 5. (a) 2D NOESY of compound 4a; (b) 2D NOESY of compound 4b.

experimentally for compounds **10b** (1.75) and **4b** (2.84). It is noteworthy to stress that all the best six hits for P-gp ( $IC_{50}$

ranking from 0.20 to 1.23  $\mu M$ ) have a 2-methoxy group on the C-ring and therefore the possibility to establish an HB seems to be a



**Figure 6.** (a–d) Probability distribution of the dihedral angle  $\phi$  during the MD trajectory in water (a) and in chloroform (b) for 4a and 4b; (c) DFT optimized molecular structure of 4b:  $\phi$  indicates the dihedral angle (rotation around the C–C bond) whose value is indicative of the intramolecular H-bond occurrence (depicted as a dotted line); (d) DFT potential energy profile for the torsion around the dihedral angle  $\phi$  in 4b.

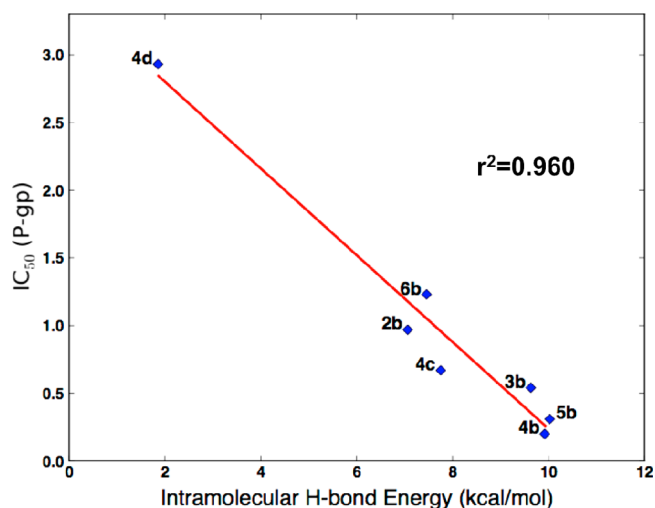


**Figure 7.** Relationship between P-gp  $IC_{50}$  and IMHB energy barrier values. All calculations were performed at the B3LYP/6-31G(d) level of theory.

molecular determinant for a high affinity. Compound 4d has two dimethoxy groups on ring C in positions 2 and 6 and the probable steric hindrance of the methoxy group with the carbonyl of the carboxamide linker likely induces an out-of-plane conformation, leading to the lack of H-bonding activity of the methoxy group with the amide NH.

The two regioisomers 4b and 5b, bearing in the A-ring a 3- or a 4-pyridinyl ring, respectively, resulted close log  $P$  values (2.84 and 3.13, respectively) and likewise of P-gp inhibitory activity

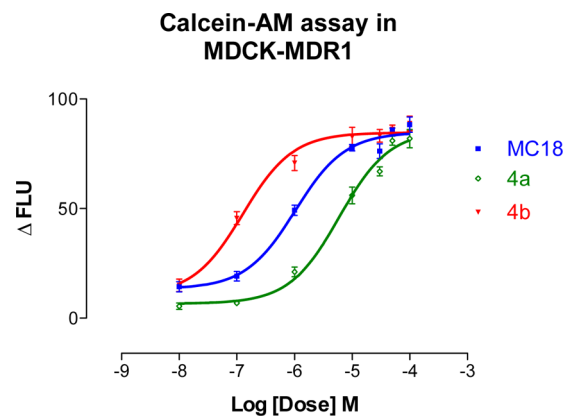


**Figure 8.** Representative curves for the MDR1 inhibitory activities of selected compounds and MC18, carried out with calcein-AM assay in MDCK-MDR1 cell lines. Each compound has been tested at seven concentrations (from 0.1 to 100  $\mu$ M), each concentration in triplicate in two independent experiments. The y-axis indicates the percentage of  $\Delta FLU$  (fluorescence units). Statistical analysis was performed with the Friedman test ( $P = 0.0078$ , significant; Friedman value equal to 11.87).

(0.20 and 0.31  $\mu$ M, respectively). On the other hand, 5b inhibited P-gp, but not MRP1 ( $IC_{50} > 100 \mu$ M), while 4b was much more active on MRP1, showing an  $IC_{50}$  of 3.38  $\mu$ M.

Concerning the inhibitory activity of compounds reported so far, a dependence from lipophilicity has never been described. Interestingly, MRP1 inhibitory activities, measurable as  $IC_{50}$  only for 11 compounds (see Table 1), were poorly correlated with the experimental log  $D_{7.4}$  values.

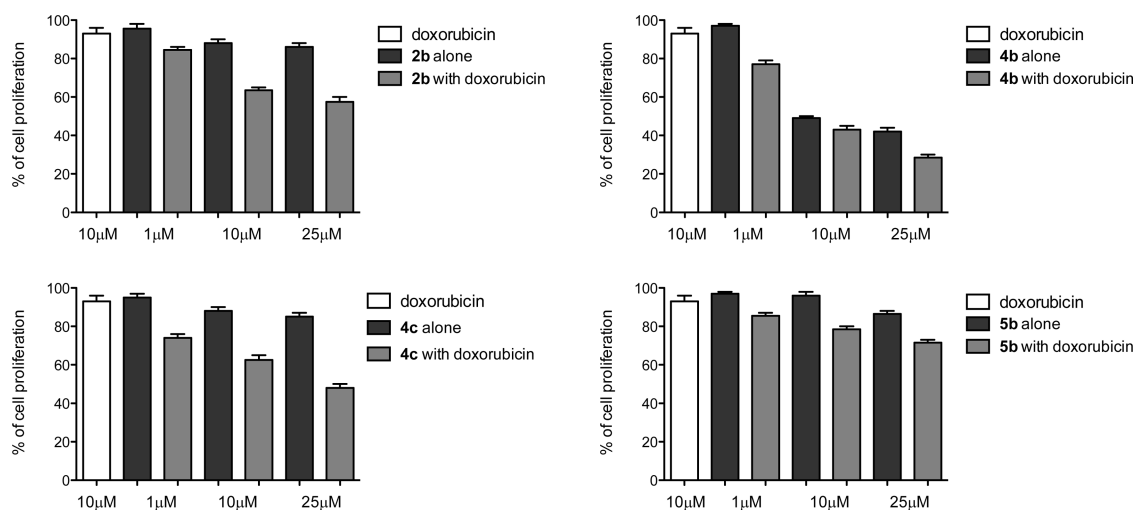


**Figure 9.** Co-administration of doxorubicin with compounds **2b**, **4b**, **4c**, and **5b**. Antiproliferative effect of 10  $\mu\text{M}$  doxorubicin (white bars) at 48 h in MCF7 adr cell line. In comparison, P-gp active compounds (1, 10, and 25  $\mu\text{M}$ ) were administered for 24 h (black bars). After washing, compounds were co-administered with doxorubicin (10  $\mu\text{M}$ ) at the same concentration for 48 h (gray bars).

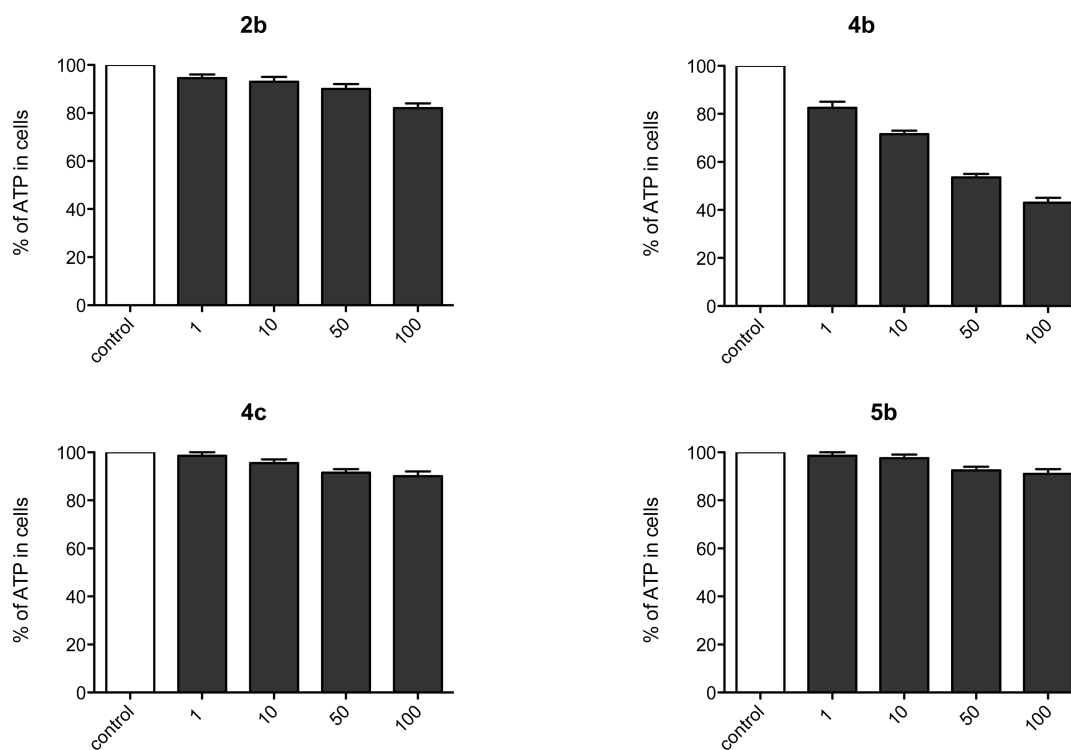


**Figure 10.** ATP consumption in MDCK-MDR1 by compounds **2b**, **4b**, **4c**, and **5b**. Control of untreated cells (white bars); cell treatment with 1, 10, 50, and 100  $\mu\text{M}$  of tested compounds (black bars).

It is noteworthy to point out that compound **9a** is the only compound of this series showing a slight selectivity for MRP1 (11.10 vs 18.50  $\mu\text{M}$ ). On the other hand, its parent compound **8a**, despite similar log  $D_{7.4}$  values, showed the usual trend (P-gp selectivity), with  $\text{IC}_{50}$  of 15.8 and 2.76  $\mu\text{M}$  on MRP1 and P-gp, respectively.

## CONCLUSIONS

P-Glycoprotein is an unusual transporter, and various aspects of its function appear to be modulated by the lipid environment in novel and complex ways. The lipophilicity of potential inhibitors should therefore be carefully considered in the molecular design

process. The relationship between modulation activity of P-gp and lipophilicity was observed and confirmed in many series of effective inhibitors. However, in many cases, high activities were shown by compounds with prohibitive solubility and log  $D$  values, compromising a possible hit-to-lead development. In this work, we demonstrate that the careful selection of regioisomers, able to form IMHBs, can result in very promising hits; 5 of 21 very small molecules, soluble in an aqueous medium at concentrations  $20 \pm 10$  mg/L (**2b**) to  $250 \pm 50$  mg/L (**3b**), showed submicromolar  $\text{IC}_{50}$  values against P-gp, and three of them are also active toward MRP1 with  $\text{IC}_{50}$  in the one-digit micromolar range. Finally, both MD simulations and DFT calculations suggest the presence of a unique conformation of the

hit **4b** characterized by a very stable IMHB, thus providing a rationale for the different activities reported for the regioisomers **4a** and **4b**. The strength of such interaction is here proved to be a sensitive parameter for a soft modulation of the P-gp response. For instance, the 2,4,5-trimethoxybenzamide derivatives **3b**, **4b**, and **5b** display the highest activity and are also characterized by the strongest IMHB.

## EXPERIMENTAL SECTION

**Chemistry.** High analytical grade chemicals and solvents were purchased from commercial suppliers. When necessary, solvents were dried by standard techniques and distilled. After extraction from aqueous layers, the organic solvents were dried over anhydrous sodium sulfate. Thin layer chromatography (TLC) was performed on aluminum sheets precoated with silica gel 60 F254 (0.2 mm) (E. Merck). Chromatographic spots were visualized by UV light. Purification of crude compounds was carried out by flash column chromatography on silica gel 60 (Kieselgel 0.040–0.063 mm, E. Merck) or by preparative TLC on silica gel 60 F254 plates or crystallization.  $^1\text{H}$  NMR spectra were recorded in DMSO- $d_6$  or  $\text{CDCl}_3$  at 300 MHz on a Varian Mercury 300 instrument. Chemical shifts ( $\delta$  scale) are reported in parts per million (ppm) relative to the central peak of the solvent. Coupling constant ( $J$  values) are given in hertz (Hz). Spin multiplicities are given as s (singlet), br s (broad singlet), d (doublet), t (triplet), dd (double doublet), dt (double triplet), or m (multiplet). LRMS (ESI) was performed with an electrospray interface ion trap mass spectrometer (1100 series LC/MSD trap system Agilent, Palo Alto, CA). In all cases, spectroscopic data are in agreement with known compounds and assigned structures. The known compounds **1a** and **1b** (Figure 1) were already published in our previous work.<sup>14</sup> Combustion analyses were performed by Eurovector Euro EA 3000 analyzer (Milan, Italy) and gave satisfactory results (C, H, N within 0.4% of calculated values). clogP values of the data set were computed by using the Bio-Loom software package version 1.5; ALOGPS values were computed by using software developed by Virtual Computational Chemistry Laboratory v. 2.1; log  $P$  values were computed using ACD/Laboratories version 6.00; log  $D$  values at pH 7.4 were obtained by octanol/PBS buffer partitioning analysis using chemiluminescent nitrogen detection method performed by Analiza Incorporated.

**Chromatographic Settings.** Log  $k'$  values and purity determinations were carried out using a Zorbax 300SB-C18 4.6 mm  $\times$  250 mm, with 5  $\mu\text{m}$  size particles, built on a Waters double pump HPLC system in isocratic conditions. Injection volumes were 5  $\mu\text{L}$ , flow rate was 1 mL/min, and detection was performed with UV ( $\lambda$  = 230 and 254 nm). Samples were prepared by dissolving 0.1 mg/mL of the solute in 10% (v/v) DMSO and 90% (v/v) methanol. Retention times ( $t_r$ ) were measured at least from three separate injections, and dead time ( $t_0$ ) was the retention time of deuterated water. The mobile phase was filtered through a Nylon-66 membrane 0.45  $\mu\text{m}$  (Supelco, USA) before use. For each reference compound, the average retention time ( $t_r$ ) of three consecutive injections of 5  $\mu\text{L}$  of sample was used to calculate the log  $k'$  values ( $\log k' = \log[(t_r - t_0)/t_0]$ ). The eluent consisted of three different mixtures of methanol and PBS buffer at pH 7.4: the first measurement was 80% (v/v) methanol and 20% (v/v) of buffer, 70% (v/v) methanol and 30% (v/v) of buffer, and 60% (v/v) methanol and 40% (v/v) of buffer.

**i. General Procedure for the Suzuki–Miyaura Cross-Coupling Reaction: Preparation of Compounds 1–6 (Scheme 1).** A suspension of the chosen aniline (5.0 mmol), the appropriated boronic acid (7.5 mmol), and  $\text{Pd}(\text{PPh}_3)_4$  (0.50 mmol) in a 2 M aqueous solution of  $\text{K}_2\text{CO}_3$  (7.5 mL) and 1,4-dioxane (30 mL) was heated at 100  $^\circ\text{C}$  for 3 h under stirring. After cooling, the solvent was evaporated under vacuum to dryness and the obtained residue was treated with dichloromethane or ethyl acetate. The suspension was filtered on Celite or silica gel, and the resulting residue was purified by chromatography.

**5-(3,5-Difluorophenyl)pyridin-2-amine (2).**<sup>32</sup> Purified by chromatography (hexane/ethyl acetate, 60:40). Yield 45%; mp 107.4–108.9  $^\circ\text{C}$ .  $^1\text{H}$  NMR ( $\text{CDCl}_3$ )  $\delta$ : 8.29 (d, 1H,  $J$  = 2.4 Hz), 7.62 (dd, 1H,  $J$  = 8.5, 2.4

Hz), 7.06–6.96 (m, 2H), 6.79–6.70 (m, 1H), 6.57 (d, 1H,  $J$  = 8.7 Hz), 4.58 (br s, 2H). LRMS (ESI)  $m/z$  204.8  $[\text{M} - \text{H}]^-$ .

**3,3'-Bipyridin-6-amine (3).**<sup>33</sup> Purified by chromatography (dichloromethane/methanol, 90:10). Yield 50%; mp 118.3–122.5  $^\circ\text{C}$ .  $^1\text{H}$  NMR ( $\text{CDCl}_3$ )  $\delta$ : 8.79–8.76 (m, 1H), 8.58–8.54 (m, 1H), 8.33–8.30 (m, 1H), 7.83–7.77 (m, 1H), 7.67 (dd, 1H,  $J$  = 8.5, 2.4 Hz), 7.37–7.31 (m, 1H), 6.61 (d, 1H,  $J$  = 8.4 Hz), 4.55 (br s, 2H). LRMS (ESI)  $m/z$  169.9  $[\text{M} - \text{H}]^-$ .

**2-Fluoro-4-(pyridin-3-yl)aniline (4).** Purified by chromatography (hexane/ethyl acetate, 50:50). Yield 90%; mp 92.5–95.4  $^\circ\text{C}$ .  $^1\text{H}$  NMR ( $\text{CDCl}_3$ )  $\delta$ : 8.79–8.76 (m, 1H), 8.54–8.50 (m, 1H), 7.81–7.76 (m, 1H), 7.33–7.16 (m, 3H), 6.90–6.82 (m, 1H), 3.85 (br s, 2H). LRMS (ESI)  $m/z$  186.9  $[\text{M} - \text{H}]^-$ .

**2-Fluoro-4-(pyridin-4-yl)aniline (5).** Purified by chromatography (ethyl acetate/hexane, 60:40). Yield 40%; mp 157.4–159.5  $^\circ\text{C}$ .  $^1\text{H}$  NMR ( $\text{DMSO}-d_6$ )  $\delta$ : 8.51–8.47 (m, 2H), 7.64–7.50 (m, 3H), 7.41 (dd, 1H,  $J$  = 8.1, 1.8 Hz), 6.86–6.80 (m, 1H), 5.56 (br s, 2H). LRMS (ESI)  $m/z$  186.9  $[\text{M} - \text{H}]^-$ .

**3-Fluoro-4'-methoxybiphenyl-4-amine (6).**<sup>34</sup> Purified by chromatography (chloroform/hexane, 80:20). Yield 30%; mp 134.8–136.5  $^\circ\text{C}$ .  $^1\text{H}$  NMR ( $\text{CDCl}_3$ )  $\delta$ : 7.47–7.41 (m, 2H), 7.21–7.17 (m, 1H), 7.16–7.13 (m, 1H), 6.97–6.92 (m, 2H), 6.86–6.78 (m, 1H), 3.84 (s, 3H), 3.73 (br s, 2H). LRMS (ESI)  $m/z$  215.8  $[\text{M} - \text{H}]^-$ .

**ii. Procedure for the Preparation of N-(2-Fluoro-4-(pyridin-3-yl)phenyl)-3,4-dimethoxybenzenesulfonamide (7j) (Scheme 1).** The aniline derivative **4** (0.50 mmol) and 3,4-dimethoxybenzene-1-sulfonyl chloride (0.75 mmol) were dissolved in a minimum volume of THF dry and stirred at room temperature for 7 h. The mixture was evaporated under vacuum to dryness and the residue purified by chromatography (ethyl acetate/hexane, 60:40) to obtain the desired product.

Yield 61%; mp 173.4–176.3  $^\circ\text{C}$ .  $^1\text{H}$  NMR ( $\text{DMSO}-d_6$ )  $\delta$ : 10.17 (s, 1H), 8.85 (m, 1H), 8.53 (d, 1H,  $J$  = 4.7 Hz), 8.03 (d, 1H,  $J$  = 8.2 Hz), 7.59 (d, 1H,  $J$  = 12.1 Hz), 7.51–7.40 (m, 2H), 7.38–7.29 (m, 2H), 7.27 (d, 1H,  $J$  = 1.8 Hz), 7.05 (d, 1H,  $J$  = 8.7 Hz), 3.78 (s, 3H), 3.72 (s, 3H). LRMS (ESI)  $m/z$  386.8  $[\text{M} - \text{H}]^-$ .

**iii. General Procedures for the Preparation of Compounds 2a, 2b, 3a, 3b, 4a–4i, 5a, 5b, and 6b (Scheme 1).** For compounds **2a**, **3a**, **4a**, **4e**, **4f**, **4h**, and **5a**, the chosen aniline (0.50 mmol) and the appropriate benzoyl chloride (0.75 mmol) were dissolved in the minimum volume of THF dry and stirred at room temperature for 6 h. The suspension obtained was filtered and the residue purified by crystallization, affording the desired product.

**N-(5-(3,5-Difluorophenyl)pyridin-2-yl)-3,4,5-trimethoxybenzamide (2a).** Crystallized from ethanol. Yield 23%; mp 171.5–173.2  $^\circ\text{C}$ .  $^1\text{H}$  NMR ( $\text{DMSO}-d_6$ )  $\delta$ : 8.79 (s, 1H), 8.81 (d, 1H,  $J$  = 1.9 Hz), 8.31–8.26 (m, 2H), 7.57 (dd, 2H,  $J$  = 7.2, 1.9 Hz), 7.42 (s, 2H), 7.25–7.22 (m, 1H), 3.86 (s, 6H), 3.72 (s, 3H). LRMS (ESI)  $m/z$  398.9  $[\text{M} - \text{H}]^-$ .

**N-([3,3'-Bipyridin]-6-yl)-3,4,5-trimethoxybenzamide (3a).** Purified by preparative TLC (dichloromethane/methanol, 94:6). Yield 10%; mp 134.3–135.9  $^\circ\text{C}$ .  $^1\text{H}$  NMR ( $\text{DMSO}-d_6$ )  $\delta$ : 10.99 (s, 1H), 8.97 (d, 1H,  $J$  = 2.0 Hz), 8.80 (d, 1H,  $J$  = 2.0 Hz), 8.59 (d, 1H,  $J$  = 6.0 Hz), 8.32 (d, 1H,  $J$  = 8.8 Hz), 8.23 (dd, 1H,  $J$  = 8.8, 2.5 Hz), 8.17 (dd, 1H,  $J$  = 6.0, 2.0 Hz), 7.52–7.46 (m, 1H), 7.42 (s, 2H), 3.87 (s, 6H), 3.72 (s, 3H). LRMS (ESI)  $m/z$  363.9  $[\text{M} - \text{H}]^-$ .

**N-(2-Fluoro-4-(pyridin-3-yl)phenyl)-3,4,5-trimethoxybenzamide (4a).** Crystallized from methanol. Yield 81%; mp 222.4–224.2  $^\circ\text{C}$ .  $^1\text{H}$  NMR ( $\text{DMSO}-d_6$ )  $\delta$ : 10.23 (s, 1H), 9.19 (d, 1H,  $J$  = 2.5 Hz), 8.78 (dd, 1H,  $J$  = 5.4, 1.2 Hz), 8.64 (d, 1H,  $J$  = 8.1 Hz), 7.91–7.89 (m, 1H), 7.87 (s, 1H), 7.80–7.71 (m, 2H), 7.34 (s, 2H), 3.89 (s, 6H), 3.73 (s, 3H). LRMS (ESI)  $m/z$  383.0  $[\text{M} + \text{H}]^+$ .

**N-(2-Fluoro-4-(pyridin-3-yl)phenyl)-3,4-dimethoxybenzamide (4e).** Crystallized from methanol. Yield 84%; mp 256.6–259.1  $^\circ\text{C}$ .  $^1\text{H}$  NMR ( $\text{DMSO}-d_6$ )  $\delta$ : 10.10 (s, 1H), 9.12 (s, 1H), 8.72 (d, 1H,  $J$  = 5.0 Hz), 8.52–8.49 (m, 1H), 7.87–7.61 (m, 5H), 7.57 (d, 1H,  $J$  = 1.8 Hz), 7.09 (d, 1H,  $J$  = 8.7 Hz), 3.83 (s, 6H). LRMS (ESI)  $m/z$  351.0  $[\text{M} - \text{H}]^-$ .

**N-(2-Fluoro-4-(pyridin-3-yl)phenyl)-3,5-dimethoxybenzamide (4f).** Crystallized from methanol. Yield 98%; mp 235.5–237.5  $^\circ\text{C}$ .  $^1\text{H}$  NMR ( $\text{DMSO}-d_6$ )  $\delta$ : 10.28 (s, 1H), 9.23 (s, 1H), 8.81 (d, 1H,  $J$  = 5.2 Hz), 8.73 (d, 1H,  $J$  = 8.3 Hz), 7.99–7.86 (m, 2H), 7.81–7.71 (m, 2H),



7.15 (d, 2H,  $J = 2.1$  Hz), 6.74–6.71 (m, 1H), 3.81 (s, 6H). LRMS (ESI)  $m/z$  353.0  $[M + H]^+$ .

**N-(2-Fluoro-4-(pyridin-3-yl)phenyl)benzamide (4h).** Crystallized from methanol. Yield 98%; mp 266.2–268.3 °C.  $^1\text{H}$  NMR (DMSO- $d_6$ )  $\delta$ : 10.30 (s, 1H), 9.20 (s, 1H), 8.79 (d, 1H,  $J = 4.4$  Hz), 8.68 (d, 1H,  $J = 8.0$  Hz), 7.99 (d, 2H,  $J = 6.2$  Hz), 7.94–7.90 (m, 1H), 7.86–7.84 (m, 1H), 7.80 (d, 1H,  $J = 8.0$  Hz), 7.75–7.70 (m, 1H), 7.63–7.50 (m, 3H). LRMS (ESI)  $m/z$  293.0  $[M + H]^+$ .

**N-(2-Fluoro-4-(pyridin-4-yl)phenyl)-3,4,5-trimethoxybenzamide (5a).** Crystallized from methanol. Yield 54%; mp 265.3–267.2 °C.  $^1\text{H}$  NMR (DMSO- $d_6$ )  $\delta$ : 10.35 (s, 1H), 8.91 (d, 2H,  $J = 6.6$  Hz), 8.35 (d, 2H,  $J = 6.6$  Hz), 8.08 (dd, 1H,  $J = 12.1, 1.9$  Hz), 7.96–7.83 (m, 2H), 7.34 (s, 2H), 3.86 (s, 6H), 3.73 (s, 3H). LRMS (ESI)  $m/z$  383.0  $[M + H]^+$ .

For compounds **2b**, **3b**, **4b**–**d**, **4g**, **5b**, and **6b**, the starting benzoic acid (0.75 mmol) was suspended under argon in thionyl chloride (1.0 mL) and stirred for 3 h at room temperature. The unreacted excess of thionyl chloride was removed under nitrogen flow to afford the corresponding benzoyl chloride. The solid obtained and the appropriate aniline (0.50 mmol) were dissolved in the minimum volume of THF dry and stirred at room temperature for 6 h. The suspension obtained was filtered and the residue was purified by crystallization, affording the desired product.

**N-(5-(3,5-Difluorophenyl)pyridin-2-yl)-2,4,5-trimethoxybenzamide (2b).** Crystallized from methanol. Yield 37%; mp 248.2–252.9 °C.  $^1\text{H}$  NMR (DMSO- $d_6$ )  $\delta$ : 10.54 (s, 1H), 8.76 (d, 1H,  $J = 2.2$  Hz), 8.35 (d, 1H,  $J = 8.5$  Hz), 8.24 (d, 1H,  $J = 8.5, 2.2$  Hz), 7.59–7.51 (m, 3H), 7.30–7.20 (m, 1H), 6.87 (s, 1H), 4.06 (s, 3H), 3.90 (s, 3H), 3.77 (s, 3H). LRMS (ESI)  $m/z$  423.1  $[M + Na]^+$ .

**N-([3,3'-Bipyridin]-6-yl)-2,4,5-trimethoxybenzamide (3b).** Crystallized from methanol. Yield 68%; mp 209.6–212.1 °C.  $^1\text{H}$  NMR (DMSO- $d_6$ )  $\delta$ : 10.53 (s, 1H), 8.95 (d, 1H,  $J = 2.3$  Hz), 8.73 (d, 1H,  $J = 2.3$  Hz), 8.58 (dd, 1H,  $J = 5.0, 1.5$  Hz), 8.37 (d, 1H,  $J = 8.8$  Hz), 8.23 (dd, 1H,  $J = 8.8, 2.5$  Hz), 8.15–8.11 (m, 1H), 7.56 (s, 1H), 7.53–7.47 (m, 1H), 6.88 (s, 1H), 4.07 (s, 3H), 3.90 (s, 3H), 3.77 (s, 3H). LRMS (ESI)  $m/z$  388.2  $[M + Na]^+$ .

**N-(2-Fluoro-4-(pyridin-3-yl)phenyl)-2,4,5-trimethoxybenzamide (4b).** Crystallized from methanol. Yield 79%; mp 256.7–260.1 °C.  $^1\text{H}$  NMR (DMSO- $d_6$ )  $\delta$ : 10.41 (d, 1H,  $J = 2.7$  Hz), 9.18 (d, 1H,  $J = 2.5$  Hz), 8.76 (d, 1H,  $J = 5.4$  Hz), 8.70 (d, 1H,  $J = 8.4$  Hz), 8.54 (t, 1H,  $J = 8.4$  Hz), 7.93–7.87 (m, 2H), 7.75 (dd, 1H,  $J = 8.7, 1.5$  Hz), 7.56 (s, 1H), 6.88 (s, 1H), 4.07 (s, 3H), 3.90 (s, 3H), 3.77 (s, 3H). LRMS (ESI)  $m/z$  405.0  $[M + Na]^+$ .

**N-(2-Fluoro-4-(pyridin-3-yl)phenyl)-2,3,4-trimethoxybenzamide (4c).** Crystallized from ethanol. Yield 56%; mp 236.7–239.0 °C.  $^1\text{H}$  NMR (DMSO- $d_6$ )  $\delta$ : 10.47 (s, 1H), 9.14 (s, 1H), 8.75–8.73 (m, 1H), 8.59–8.52 (m, 1H), 8.46 (t, 1H,  $J = 8.4$  Hz), 7.91 (d, 1H,  $J = 12.9$  Hz), 7.86–7.80 (m, 1H), 7.75 (d, 1H,  $J = 8.9$  Hz), 7.74–7.72 (m, 1H), 7.02 (d, 1H,  $J = 8.9$  Hz), 4.02 (s, 3H), 3.88 (s, 3H), 3.80 (s, 3H). LRMS (ESI)  $m/z$  405.1  $[M + Na]^+$ .

**N-(2-Fluoro-4-(pyridin-3-yl)phenyl)-2,4,6-trimethoxybenzamide (4d).** Crystallized from methanol. Yield 10%; mp 189.6–191.0 °C.  $^1\text{H}$  NMR (DMSO- $d_6$ )  $\delta$ : 9.91 (s, 1H), 8.92 (d, 1H,  $J = 2.2$  Hz), 8.55 (dd, 1H,  $J = 4.7, 1.6$  Hz), 8.14–8.08 (m, 2H), 7.67 (dd, 1H,  $J = 12.1, 1.6$  Hz), 7.57 (d, 1H,  $J = 8.2$  Hz), 7.47 (dd, 1H,  $J = 8.2, 4.7$  Hz), 6.27 (s, 2H), 3.74 (s, 3H), 3.30 (s, 6H). LRMS (ESI)  $m/z$  405.2  $[M + Na]^+$ .

**N-(2-Fluoro-4-(pyridin-3-yl)phenyl)-4-methoxybenzamide (4g).** Crystallized from methanol. Yield 69%; mp 271.2–272.7 °C.  $^1\text{H}$  NMR (DMSO- $d_6$ )  $\delta$ : 10.12 (s, 1H), 9.17 (s, 1H), 8.77 (d, 1H,  $J = 5.2$  Hz), 8.63 (d, 1H,  $J = 8.1$  Hz), 7.98 (d, 2H,  $J = 8.5$  Hz), 7.92–7.82 (m, 2H), 7.78 (d, 1H,  $J = 8.1$  Hz), 7.70 (d, 1H,  $J = 8.4$  Hz), 7.06 (d, 2H,  $J = 8.5$  Hz), 3.83 (s, 3H). LRMS (ESI)  $m/z$  323.2  $[M + H]^+$ .

**N-(2-Fluoro-4-(pyridin-4-yl)phenyl)-2,4,5-trimethoxybenzamide (5b).** Crystallized from methanol. Yield 58%; mp 247.7–251.5 °C.  $^1\text{H}$  NMR (DMSO- $d_6$ )  $\delta$ : 10.52 (d, 1H,  $J = 3.0$  Hz), 8.84 (d, 2H,  $J = 6.0$  Hz), 8.60 (t, 1H,  $J = 8.5$  Hz), 8.24 (d, 2H,  $J = 6.0$  Hz), 8.09 (dd, 1H,  $J = 11.3, 1.9$  Hz), 7.93 (d, 1H,  $J = 11.3$  Hz), 7.55 (s, 1H), 6.89 (s, 1H), 4.09 (s, 3H), 3.90 (s, 3H), 3.78 (s, 3H). LRMS (ESI)  $m/z$  405.1  $[M + Na]^+$ .

**N-(3-Fluoro-4'-methoxy-[1,1'-biphenyl]-4-yl)-2,4,5-trimethoxybenzamide (6b).** Purified by chromatography (hexane/ethyl acetate, 50:50). Yield 87%; mp 157.8–160.3 °C.  $^1\text{H}$  NMR (CDCl<sub>3</sub>)  $\delta$ : 10.40–

10.38 (m, 1H), 8.66–8.59 (m, 1H), 7.83 (s, 1H), 7.55–7.49 (m, 2H), 7.39–7.28 (m, 2H), 7.00–6.95 (m, 2H), 6.59 (s, 1H), 4.08 (s, 3H), 3.98 (s, 3H), 3.94 (s, 3H), 3.85 (s, 3H). LRMS (ESI)  $m/z$  434.2  $[M + Na]^+$ .

**N-(2-Fluoro-4-(pyridin-3-yl)phenyl)nicotinamide (4i).** A suspension of **4** (0.50 mmol), nicotinoyl chloride hydrochloride (0.75 mmol), DMAP (0.50 mmol), and Et<sub>3</sub>N (1.0 mmol) in 1,4-dioxane (3.0 mL) was heated at 100 °C under stirring for 2 h, then the mixture was evaporated to dryness and the desired compound was purified by chromatography (dichloromethane/methanol, 95:5). Yield 77%; mp 165.4–166.7 °C.  $^1\text{H}$  NMR (DMSO- $d_6$ )  $\delta$ : 10.44 (s, 1H), 9.12 (d, 1H,  $J = 1.7$  Hz), 8.95 (d, 1H,  $J = 1.7$  Hz), 8.77 (dd, 1H,  $J = 4.7, 1.7$  Hz), 8.57 (dd, 1H,  $J = 4.7, 1.7$  Hz), 8.31 (dt, 1H,  $J = 8.5, 1.7$  Hz), 8.16–8.12 (m, 1H), 7.80–7.74 (m, 2H), 7.66–7.54 (m, 2H), 7.54–7.47 (m, 1H). LRMS (ESI)  $m/z$  291.9  $[M - H]^-$ .

**iv. General Procedure for Preparation of Compounds 10a and 10b (Scheme 1).** The chosen benzamide **4a** or **4b** (0.30 mmol) and sodium hydride (0.33 mmol) were suspended in DMF dry (15 mL) at 0 °C and stirred for 30 min. Methyl iodide (0.33 mmol) was added, and the reaction was allowed to warm to room temperature. After 3 h, the reaction was quenched with ice. The organic phase was extracted with dichloromethane, dried over anhydrous sodium sulfate, and evaporated under vacuum to dryness. The residue was purified by chromatography, affording the desired product.

**N-(2-Fluoro-4-(pyridin-3-yl)phenyl)-3,4,5-trimethoxy-N-methylbenzamide (10a).** Purified by chromatography (ethyl acetate/hexane, 80:20). Yield 68%; mp 97.8–102.2 °C.  $^1\text{H}$  NMR (CDCl<sub>3</sub>)  $\delta$ : 8.82–8.76 (m, 1H), 8.67–8.61 (m, 1H), 7.85–7.80 (m, 1H), 7.45–7.36 (m, 1H), 7.35–7.25 (m, 2H), 7.22–7.13 (m, 1H), 6.63 (s, 2H), 3.79 (s, 3H), 3.69 (s, 6H), 3.45 (s, 3H). LRMS (ESI)  $m/z$  419.2  $[M + Na]^+$ .

**N-(2-Fluoro-4-(pyridin-3-yl)phenyl)-2,4,5-trimethoxy-N-methylbenzamide (10b).** Purified by chromatography (ethyl acetate/hexane, 90:10). Yield 19%; mp 102.7–105.3 °C.  $^1\text{H}$  NMR (CDCl<sub>3</sub>)  $\delta$ : 8.76 (s, 1H), 8.60 (d, 1H,  $J = 4.4$  Hz), 7.78 (d, 1H,  $J = 8.3$  Hz), 7.40–7.25 (m, 2H), 7.17–7.06 (m, 2H), 6.91 (s, 1H), 6.20 (s, 1H), 3.80 (s, 6H), 3.61 (s, 3H), 3.44 (s, 3H). LRMS (ESI)  $m/z$  419.2  $[M + Na]^+$ .

**v. Procedure for the Preparation of N-(3-Amino-3',5'-difluoro-[1,1'-biphenyl]-4-yl)-3,4,5-trimethoxybenzamide (8a) (Scheme 1).** A suspension of the benzamide **1a** (0.20 mmol) in absolute ethanol (25 mL) was stirred at room temperature with a catalytic amount of Pd/C (5% w/w) under H<sub>2</sub> atmosphere. After 2 h, the suspension was filtered on syringe filter (Filték RC, pore size 0.20  $\mu\text{m}$ ) to remove the catalyst. The filtrate was evaporated under vacuum to dryness affording the desired product.

Yield 91%; mp 219.8–222.2 °C.  $^1\text{H}$  NMR (DMSO- $d_6$ )  $\delta$ : 9.70 (s, 1H), 7.39–7.13 (m, 7H), 6.97 (dd, 1H,  $J = 8.2, 1.9$  Hz), 5.04 (br s, 2H), 3.85 (s, 6H), 3.71 (s, 3H). LRMS (ESI)  $m/z$  412.9  $[M - H]^-$ .

**vi. Procedure for the Preparation of N-(3-(2-Acetamidopropionamido)-3',5'-difluoro-[1,1'-biphenyl]-4-yl)-3,4,5-trimethoxybenzamide (9a) (Scheme 1).** The benzamide **8a** (0.18 mmol) was dissolved in THF dry and *N*-acetyl-L-alanine (0.15 mmol), EDC (0.18 mmol), HOBt (0.18 mmol), and TEA (0.36 mmol) were added. The mixture was stirred at room temperature for 72 h. The suspension obtained was filtered and the filtrate evaporated under vacuum to dryness. The desired product was purified by chromatography (dichloromethane/methanol, 98:2). Yield 32%; mp 196.4–200.9 °C.  $^1\text{H}$  NMR (DMSO- $d_6$ )  $\delta$ : 9.93 (s, 1H), 9.58 (s, 1H), 8.30 (d, 1H,  $J = 6.9$  Hz), 7.95 (d, 1H,  $J = 1.9$  Hz), 7.70 (d, 1H,  $J = 8.5$  Hz), 7.61 (dd, 1H,  $J = 6.0$  Hz), 7.41 (m, 2H), 7.32 (s, 2H), 7.27–7.21 (m, 1H), 4.37–4.33 (m, 1H), 3.86 (s, 6H), 3.72 (s, 3H), 1.74 (s, 3H), 1.30 (d, 3H,  $J = 7.2$  Hz). LRMS (ESI)  $m/z$  526.2  $[M - H]^-$ .

**Computational Studies.** Classical molecular dynamics (MD) simulations were carried out with the NAMD 2.9 software.<sup>35</sup> For compounds **4a** and **4b**, the CHARMM General Force Field (CGenFF) force field parameters<sup>36</sup> were used and the atomic charges were calculated with the Restrained Electrostatic Potential (RESP) approach<sup>37</sup> using Jaguar 7.6 software.<sup>38</sup> TIP3P model<sup>39</sup> was used for explicit water solvent, while chloroform was simulated using the OPLS-AA<sup>40</sup> force field. A time step of 1 fs was used; data were sampled every 100 fs. The investigated systems were first equilibrated for 0.5 ns at 310 K; then, data were sampled over a 5 ns trajectory at the same temperature. All simulations were performed in the canonical ensemble.



All DFT calculations were carried out using Jaguar 7.6 software. Geometry optimizations and relaxed scan calculations were performed at the B3LYP/6-31G(d)<sup>41</sup> level. Harmonic vibrational frequency analyses were applied in order to confirm the nature of the localized stationary states.

**Biology. Materials.** ATPlite 1 step kit and CulturePlate 96-well plates were purchased from PerkinElmer Life and Analytical Sciences (Boston, MA, USA). Cell culture reagents were obtained from EuroClone (Milan, Italy). Calcein-AM, MTT (3-[4,5-dimethylthiazol-2-yl]-2,5-diphenyltetrazolium bromide), and doxorubicin were obtained from Sigma-Aldrich (Milan, Italy).

**Cell Cultures.** Human MCF7adr breast adenocarcinoma cells (resistant to doxorubicin) were kindly provided by Prof. G. Zupi (IRE, Rome, Italy), and MDCK-MDR1 and MDCK-MRP1 cells were a gift of Prof. P. Borst (NKI-AVL Institute, Amsterdam, Nederland). Caco-2 cells were kindly donated by IRCCS "S. De Bellis" (Castellana Grotte, Bari, Italy). MCF7adr cells were grown in RPMI 1640 supplemented with 10% fetal bovine serum, 2 mM glutamine, 100 U/mL penicillin, and 100 µg/mL streptomycin in a humidified incubator at 37 °C with a 5% CO<sub>2</sub> atmosphere. MDCK-MDR1, MDCK-MRP1, and Caco-2 cells were grown in DMEM high glucose supplemented with 10% fetal bovine serum, 2 mM glutamine, 100 U/mL penicillin, and 100 µg/mL streptomycin in a humidified incubator at 37 °C with a 5% CO<sub>2</sub> atmosphere.

**Co-administration Assay.** The co-administration assay with doxorubicin was performed in MCF7adr cells at 72 h.<sup>42</sup> On day 1, 25000 cells/well were seeded into 96-well plates in a volume of 100 µL. On day 2, three drug concentrations (1, 10, and 25 µM) were added. On day 3, the medium was removed and the three drugs concentrations were added alone and in combination with doxorubicin 10 µM. After the established incubation time with drugs, MTT (0.5 mg/mL) was added to each well, and after 3–4 h incubation at 37 °C, the supernatant was removed. The formazan crystals were solubilized using 100 µL of DMSO/EtOH (1:1), and the absorbance values at 570 and 630 nm were determined on the microplate reader Victor 3 from PerkinElmer Life Sciences.

**Calcein-AM Experiment.** These experiments were carried out as described by Feng et al. with minor modifications.<sup>27</sup> Calcein-AM is a profluorescent probe and is a P-gp substrate. In cells overexpressing P-gp or MRP1, Calcein-AM is not able to permeate cell membrane whereas when the efflux pump is not present or is inhibited, the probe enters living cells and is converted to fluorescent Calcein by intracellular esterases. Calcein is not able to diffuse through the membrane because it is hydrophilic and is not a P-gp or MRP1 substrate; thus, calcein accumulates in cells when the pump is blocked. Therefore, the fluorescent signal is directly correlated to the amount of P-gp or MRP1 interaction. MDCK-MDR1 or MDCK-MRP1 cells (50000 cells per well) were seeded into black CulturePlate 96-well plates with 100 µL of medium and allowed to become confluent overnight. Then 100 µL of test compounds were solubilized in culture medium and added to monolayers. The 96-well plates was incubated at 37 °C for 30 min. Calcein-AM was added in 100 µL of phosphate buffered saline (PBS) to yield a final concentration of 2.5 µM, and the plate was incubated for 30 min. Each well was washed 3 times with ice-cold PBS. Saline buffer was added to each well, and the plate was read to Victor3 (PerkinElmer) at excitation and emission wavelengths of 485 and 535 nm, respectively. In these experimental conditions calcein cell accumulation in the absence and in the presence of tested compounds was evaluated and fluorescence basal level was estimated by untreated cells. In treated wells, the increase of fluorescence with respect to basal level was measured. IC<sub>50</sub> values were determined by fitting the fluorescence increase percentage versus log[dose].

**Bioluminescent ATP Assay.** This experiment was performed as reported in technical sheet of ATPlite 1 step kit for luminescence ATP detection based on firefly (*Photinus pyralis*) luciferase (PerkinElmer Life Sciences). The ATPlite assay is based on the production of light caused by the reaction of ATP with added luciferase and D-luciferin (substrate solution), and the emitted light is proportional to the ATP concentration.<sup>43</sup> The MDCK-MDR1 cells was seeded into black CulturePlate 96-well plates in 100 µL of complete medium at a density

2 × 10<sup>4</sup> cells/well. The plate was incubated O/N in a humidified atmosphere 5% CO<sub>2</sub> at 37 °C. The medium was removed, and 100 µL of complete medium in the presence or absence of different concentrations of test compounds was added. The plate was incubated for 2 h in a humidified atmosphere 5% CO<sub>2</sub> at 37 °C. Then, 50 µL of mammalian cell lysis solution was added to all wells and the plate stirred for 5 min in an orbital shaker. In all wells, 50 µL of substrate solution was added and the plate stirred for 5 min in an orbital shaker. The plate was dark adapted for 10 min, and the luminescence was measured on the microplate reader Victor 3 from PerkinElmer Life Sciences.

**Permeability Experiment.** The preparation of Caco-2 monolayer has been previously reported by Leopoldo et al.<sup>44</sup> Apical to basolateral ( $P_{app}$ , A–B) and basolateral to apical ( $P_{app}$ , B–A) permeability of drugs were measured at 120 min and at various drug concentrations (1–100 µM). Drugs were dissolved in Hanks' Balanced Salt Solution (HBSS, pH 7.4) and sterile filtered. After 21 days of cell growth, the medium was removed from filter wells and from the receiver plate. The filter wells were filled with 75 µL of fresh HBSS buffer and the receiver plate with 250 µL per well of the same buffer. This procedure was repeated twice, and the plates were incubated at 37 °C for 30 min. After incubation time, the HBSS buffer was removed and drug solutions added to the filter well (75 µL). HBSS without the drug was added to the receiver plate (250 µL). The plates were incubated at 37 °C for 120 min. After incubation time, samples were removed from the apical (filter well) and basolateral (receiver plate) side of the monolayer and then were stored in a freezer (–20 °C) pending analysis. The concentration of compounds was measured using UV spectroscopy. The apparent permeability ( $P_{app}$ ), in units of nm per s, was calculated using the following equation:

$$P_{app} = \left( \frac{V_A}{\text{Area} \times \text{time}} \right) \times \left( \frac{[\text{drug}]_{\text{acceptor}}}{[\text{drug}]_{\text{initial}}} \right)$$

where  $V_A$  is the volume (in µL) in the acceptor well; Area is the surface area of the membrane (0.11 cm<sup>2</sup> of the well); time is the total transport time in seconds (7200 s);  $[\text{drug}]_{\text{acceptor}}$  is the concentration of the drug measured by ESI-MS analyses or UV spectroscopy;  $[\text{drug}]_{\text{initial}}$  is the initial drug concentration (1 × 10<sup>–4</sup> M) in the apical or basolateral wells.

## AUTHOR INFORMATION

### Corresponding Authors

\*For S.C.: phone, +39-080-5442090; fax, +39-080-5442230; E-mail, saverio.cellamare@uniba.it.

\*for N.A.C.: phone, +39-080-5442727; fax, +39-080-5442231; E-mail, nicolaantonio.colabufo@uniba.it.

### Notes

The authors declare no competing financial interest.

## ABBREVIATIONS USED

MDR, multidrug resistance; ABC, ATP-binding cassette; P-gp, ABCB1, MDR1, P-glycoprotein; MRP1, ABCC1, human multidrug resistance associate-protein 1; lipophilicity; IMHB, intramolecular hydrogen bond; DFT, density functional theory

## REFERENCES

- (1) Baguley, B. C. Multidrug Resistance in Cancer. *Methods Mol. Biol.* **2010**, 596, 1–14.
- (2) Eckford, P. D.; Sharom, F. J. ABC Efflux Pump-Based Resistance to Chemotherapy Drugs. *Chem. Rev.* **2009**, 109, 2989–3011.
- (3) Colabufo, N. A.; Berardi, F.; Contino, M.; Niso, M.; Perrone, R. ABC Pumps and Their Role in Active Drug Transport. *Curr. Top. Med. Chem.* **2009**, 9, 119–129.
- (4) Clay, A. T.; Sharom, J. F. Lipid Bilayer Properties Control Membrane Partitioning, Binding, and Transport of P-Glycoprotein Substrates. *Biochemistry* **2013**, 52, 343–354.
- (5) Sauna, Z. E.; Ambudkar, S. V.; About, A. Switch: How P-Glycoprotein (ABCB1) Harnesses the Energy of ATP Binding and Hydrolysis to Do Mechanical Work. *Mol. Cancer Ther.* **2007**, 6, 13–23.

- (6) Szakacs, G.; Paterson, J. K.; Ludwig, J. A.; Booth-Genthe, C.; Gottesman, M. M. Targeting Multidrug Resistance in Cancer. *Nature Rev. Drug Discovery* **2006**, *5*, 219–234.
- (7) Colabufo, N. A.; Berardi, F.; Cantore, M.; Contino, M.; Inglese, C.; Niso, M.; Perrone, R. Perspectives of P-Glycoprotein Modulating Agents in Oncology and Neurodegenerative Diseases: Pharmaceutical, Biological, and Diagnostic Potentials. *J. Med. Chem.* **2010**, *53*, 1883–1897.
- (8) Jin, M. S.; Oldham, M. L.; Zhang, Q.; Chen, J. Crystal Structure of the Multidrug Transporter P-Glycoprotein from *Caenorhabditis elegans*. *Nature* **2012**, *490*, 566–569.
- (9) Palmeira, A.; Sousa, E.; Vasconcelos, M. H.; Pinto, M. M. Three Decades of P-gp Inhibitors: Skimming through Several Generations and Scaffolds. *Curr. Med. Chem.* **2012**, *19*, 1946–2025.
- (10) Kuhnle, M.; Egger, M.; Muller, C.; Mahringer, A.; Bernhardt, G.; Fricker, G.; Konig, B.; Buschauer, A. Potent and Selective Inhibitors of Breast Cancer Resistance Protein (ABCG2) Derived from the P-glycoprotein (ABCB1) Modulator Tariquidar. *J. Med. Chem.* **2009**, *52*, 1190–1197.
- (11) Klepsch, F.; Chiba, P.; Ecker, G. F. Exhaustive Sampling of Docking Poses Reveals Binding Hypotheses for Propafenone Type Inhibitors of P-Glycoprotein. *PLoS Comput. Biol.* **2011**, *7*, e1002036.
- (12) Jabeen, I.; Pleban, K.; Rinner, U.; Chiba, P.; Ecker, G. F. Structure–Activity Relationships, Ligand Efficiency, and Lipophilic Efficiency Profiles of Benzophenone-Type Inhibitors of the Multidrug Transporter P-Glycoprotein. *J. Med. Chem.* **2012**, *55*, 3261–3273.
- (13) Aller, S. G.; Yu, J.; Ward, A.; Weng, Y.; Chittaboina, S.; Zhuo, R.; Harrell, P. M.; Trinh, Y. T.; Zhang, Q.; Urbatsch, I. L.; Chang, G. Structure of P-Glycoprotein Reveals a Molecular Basis for Poly-Specific Drug Binding. *Science* **2009**, *323*, 1718–1722.
- (14) Pellicani, R. Z.; Stefanachi, A.; Niso, M.; Carotti, A.; Leonetti, F.; Nicolotti, O.; Perrone, R.; Berardi, F.; Cellamare, S.; Colabufo, N. A. Potent Galloyl-Based Selective Modulators Targeting Multidrug Resistance Associated Protein 1 and P-glycoprotein. *J. Med. Chem.* **2012**, *55*, 424–436.
- (15) According to Lipinski, C. A. Drug-Like Properties And The Causes Of Poor Solubility And Poor Permeability. *J. Pharmacol. Toxicol. Methods* **2000**, *44*, 235–249. The turbidimetric solubility assay was conducted in 96-well, flat-bottom, transparent polystyrene plates. Serial dilutions of a DMSO 1mM stock solution of test compound (SS), were prepared. As currently practiced, 2  $\mu$ L of SS were added to a 198  $\mu$ L of 100 mM PBS buffer (pH 7.4) to give a final DMSO concentration of 1% in each well and a final test compound concentration range between 1 and 500  $\mu$ g/L. Three replicates were prepared per concentration. After a 30 min incubation time, to avoid precipitation that could affect the biochemical outcomes, the absorbance is measured at 500, 550, 600, 650, and 700 nm.
- (16) Shalaeva, M.; Caron, G.; Abramov, Y. A.; O'Connell, T. N.; Plummer, M. S.; Yalamanchi, G.; Farley, K. A.; Goetz, G. H.; Philippe, L.; Shapiro, M. J. Integrating Intramolecular Hydrogen Bonding (IMHB) Considerations in Drug Discovery Using  $\Delta$ log *P* as a Tool. *J. Med. Chem.* **2013**, *56*, 4870–4879.
- (17) Bissantz, C.; Kuhn, B.; Stahl, M. A Medicinal Chemist's Guide to Molecular Interaction. *J. Med. Chem.* **2010**, *53*, S061–S084.
- (18) Over, B.; McCarren, P.; Artursson, P.; Foley, M.; Giordanetto, F.; Grünberg, G.; Hilgendorf, C.; Lee, M. D.; Matsson, P.; Muncipinto, G.; Pellissón, M.; Perry, M. W. D.; Svensson, R.; Duvall, J. R.; Kihlberg, J. Impact of Stereospecific Intramolecular Hydrogen-Bonding on Cell Permeability and Physicochemical Properties. *J. Med. Chem.* **2014**, *57*, 2746–2754.
- (19) Virtual Computational Chemistry Laboratory; Virtual Computational Chemistry Laboratory, 2005; <http://www.vcclab.org>.
- (20) Tetko, I. V.; Gasteiger, J.; Todeschini, R.; Mauri, A.; Livingstone, D.; Ertl, P.; Palyulin, V. A.; Radchenko, E. V.; Zefirov, N. S.; Makarenko, A. S.; Tanchuk, V. Y.; Prokopenko, V. V. Virtual Computational Chemistry Laboratory Design And Description. *J. Comput.-Aided Mol. Des.* **2005**, *19*, 453–463.
- (21) Analiza; Analiza, Inc.: Cleveland, OH, <http://analiza.com/index.html>.
- (22) De Marco, A.; de Candia, M.; Carotti, A.; Cellamare, S.; De Candia, E.; Altomare, C. Lipophilicity-Related Inhibition of Blood Platelet Aggregation by Nipecotin Acid Anilides. *Eur. J. Pharm. Sci.* **2004**, *22*, 153–164.
- (23) Baxter, N. J.; Williamson, M. P. Temperature Dependence Of  $^1\text{H}$  Chemical Shifts In Proteins. *J. Biomol. NMR* **1997**, *9*, 359–369.
- (24) Kovacs, H.; Mark, A.-E.; Johansson, J.; Van Gunsteren, W.-F. The Effect of Environment on the Stability of an Integral Membrane Helix: Molecular Dynamics Simulations of Surfactant Protein C in Chloroform, Methanol And Water. *J. Mol. Biol.* **1995**, *247*, 808–822.
- (25) Mottamal, M.; Shen, S.; Guembe, C.; Krilov, G. Solvation of Transmembrane Proteins by Isotropic Membrane Mimetics: A Molecular Dynamics Study. *J. Phys. Chem. B* **2007**, *111*, 11285–11296.
- (26) Alex, A.; Millan, D. S.; Perez, M.; Wakenhut, F.; Whitlock, G. A. Intramolecular Hydrogen Bonding to Improve Membrane Permeability and Absorption in beyond Rule of Five Chemical Space. *MedChemComm* **2011**, *2*, 669–674.
- (27) Feng, B.; Mills, J. B.; Davidson, R. E.; Mireles, R. J.; Janiszewski, J. S.; Troutman, M. D.; de Moraes, S. M. In Vitro P-glycoprotein Assays to Predict the in Vivo Interactions of P-glycoprotein with Drugs in the Central Nervous System. *Drug Metab. Dispos.* **2008**, *36*, 268–275.
- (28) Colabufo, N. A.; Berardi, F.; Cantore, M.; Perrone, M. G.; Contino, M.; Inglese, C.; Niso, M.; Perrone, R.; Azzariti, A.; Simone, G. M.; Paradiso, A. 4-Biphenyl and 2-Naphthyl Substituted 6,7-Dimethoxytetrahydroisoquinoline Derivatives as Potent P-gp Modulators. *Bioorg. Med. Chem.* **2008**, *16*, 3732–3743.
- (29) Polli, J. W.; Wring, S. A.; Humphreys, J. E.; Huang, L.; Morgan, J. B.; Webster, L. O.; Serabjit-Singh, C. S. Rational Use of in Vitro P-glycoprotein Assays in Drug Discovery. *J. Pharmacol. Exp. Ther.* **2001**, *299*, 620–628.
- (30) Carrupt, P.-A.; Testa, B.; Bechalany, A.; El Tayar, N.; Descas, P.; Perrissoud, D. Morphine 6-Glucuronide and Morphine 3-Glucuronide as Molecular Chameleons with Unexpected Lipophilicity. *J. Med. Chem.* **1991**, *34*, 1272–1275.
- (31) Caron, G.; Steyaert, G.; Pagliara, A.; Reymond, F.; Crivori, P.; Gaillard, P.; Carrupt, P. A.; Avdeef, A.; Comer, J. E.; Box, K. J.; Girault, H. H.; Testa, B. Structure–Lipophilicity Relationships of Neutral and Protonated B-Blockers. Part I. Intra- and Intermolecular Effects in Isotropic Solvent Systems. *Helv. Chim. Acta* **1999**, *82*, 1211–1222.
- (32) Stamford, A. W.; Dong, Y. Heteroaryl Urea Neuropeptide Y Y5 Receptor Antagonists. Int. Patent Appl. PCT/US01/49302, 2002.
- (33) Billingsley, K. L.; Anderson, K. W.; Buchwald, S. L. A Highly Active Catalyst for Suzuki–Miyaura Cross-Coupling Reactions of Heteroaryl Compounds. *Angew. Chem., Int. Ed.* **2006**, *45*, 3484–3488.
- (34) Fujimoto, R. A.; McQuire, L. W.; Monovich, L. G.; Mugrage, B. B.; Parker, D. T.; Van Duzer, J. H.; Wattanasin, S. Int. Patent Appl. PCT/EP2003/013246, 2004.
- (35) Phillips, J.-C.; Braun, R.; Wang, W.; Gumbart, J.; Tajkhorshid, E.; Villa, E.; Chipot, C.; Skeel, R.-D.; Kalé, L.; Schulten, K. Scalable Molecular Dynamics with NAMD. *J. Comput. Chem.* **2005**, *26*, 1781–1802.
- (36) K. Vanommeslaeghe, K.; Hatcher, E.; Acharya, C.; Kundu, S.; Zhong, S.; Shim, J.; Darian, E.; Guvench, O.; Lopes, P.; Vorobyov, I.; MacKerell, A.-D., Jr. CHARMM General Force Field: A Force Field for Drug-Like Molecules Compatible with the CHARMM All-Atom Additive Biological Force Fields. *J. Comput. Chem.* **2010**, *31*, 671–690.
- (37) Bayly, C.-I.; Cieplak, P.; Cornell, W.-D.; Kollman, P.-A. A Well-Behaved Electrostatic Potential Based Method Using Charge Restraints for Determining Atom-Centered Charges: The RESP Model. *J. Phys. Chem.* **1993**, *97*, 10269–10280.
- (38) Jaguar, version 7.6; Schrödinger, LLC: New York, 2009.
- (39) Jorgensen, W.-L.; Chandrasekhar, J.; Madura, J.-D.; Impey, R.-W.; Klein, M.-L. Comparison Of Simple Potential Functions For Simulating Liquid Water. *J. Chem. Phys.* **1983**, *79*, 926–935.
- (40) Jorgensen, W.-L.; Tirado-Rives, J. The OPLS Force Field for Proteins. Energy Minimizations for Crystals of Cyclic Peptides and Crambin. *J. Am. Chem. Soc.* **1988**, *110*, 1657–1666.
- (41) Becke, A.-D. Density-Functional Thermochemistry. III. The Role of Exact Exchange. *J. Chem. Phys.* **1993**, *98*, S648–S652.

(42) Azzariti, A.; Colabufo, N. A.; Berardi, F.; Porcelli, L.; Niso, M.; Simone, M. G.; Perrone, R.; Paradiso, A. Cyclohexylpiperazine Derivative PB28, A  $\sigma_2$  Agonist and  $\sigma_1$  Antagonist Receptor Inhibits Cell Growth, Modulates P-glycoprotein, and Synergizes with Anthracyclines in Breast Cancer. *Mol. Cancer Ther.* **2006**, *5*, 1807–1816.

(43) Kangas, L.; Groönroos, M.; Nieminen, A. L. Bioluminescence of Cellular ATP: A New Method for Evaluating Cytotoxic Agents in Vitro. *Med. Biol.* **1984**, *62*, 338–343.

(44) Leopoldo, M.; Lacivita, E.; De Giorgio, P.; Colabufo, N. A.; Niso, M.; Berardi, F.; Perrone, R. Design, Synthesis, and Binding Affinities of Potential Positron Emission Tomography (PET) Ligands for Visualization of Brain Dopamine D3 Receptors. *J. Med. Chem.* **2006**, *49*, 358–365.